CHAPTER 6

Computational Design of Peptide Inhibitors targeting the SARS-CoV-2 Main Protease

Computational Design of Peptide Inhibitors targeting the SARS-CoV-2 Main Protease

6.1. Abstract:

The novel coronavirus disease also known as COVID-19 caused by the severe acute respiratory syndrome coronavirus 2 (SARS-CoV-2) which was first detected in December 2019 in Wuhan, China and its effect can still be seen in some parts of the globe due to the lack of globally approved antiviral drugs for treatment and vaccines for controlling the pandemic. Chymotrypsin-like protease (3CLpro), also known as the main protease (Mpro) of SARS-CoV-2 plays a vital role during its replication process of the pathogen's lifecycle and therefore considered as a potential drug target for COVID-19. Hence targeting the Mpro is an appealing approach for drug development because of its significant role in the viral replication and transcription. Researchers have conducted numerous studies so far and confirmed that 3CLpro can act as an attractive drug target to combat COVID-19. Although small molecules dominate the field of drug market so far, peptide inhibitors still represent a class of promising candidates because of their similarity to endogenous ligand, high affinity, and low toxicity. It has been validated that therapeutic peptides can effectively and selectively inhibit the protein-protein interactions in viruses. Hence it is necessary to design potential peptide inhibitors in order to inhibit the impact of the disease. This study involves development of potential target peptides that can act against the Mpro in a competitive mode against histone deacetylase (HDAC2) which had a high-confidence interaction with Mpro. Based on the interaction between Mpro and HDAC2, 13 peptides were designed out of which based on toxicity, binding affinity and binding site prediction, two peptides (peptide2 and peptide4) were screened and subjected to MD simulation. Our study shows that the two peptides bind to the active site of the Mpro and it attains a higher stability upon binding to the peptides. We also found out that the Mpro have a strong binding affinity with both the peptides (GB_{TOT} = -72.85 kcal/mol for Mpro-peptide2 complex and GB_{TOT} = -46.36 kcal/mol for the Mpro-peptide4 complex).

6.2. Introduction:

With rising levels of transmissibility and infectivity the Coronavirus disease 2019 (COVID-19) caused by severe acute respiratory syndrome coronavirus 2 (SARS-CoV-2), has strained human health and public safety worldwide [1]. According to the World Health Organization (WHO), the COVID-19 pandemic has resulted in more than 703,874,696 confirmed cases and more than 6,965,332 confirmed deaths by March 2024 [2]. In the recent past the world faced the significant social, economic, and political chaos due to the COVID-19 disease. Due to the lack of globally approved antiviral drugs for

treatment and vaccines against the pandemic, the number of cases and/or mortalities are still being observed in some part of the globe. Supportive treatment and the use of repurposed drugs are the mainstays of current patient therapy [3]. The scientific community is now searching rapidly for efficient antiviral therapeutic methods in response to the present pandemic situation. Computational techniques are one of the most extensively used approaches for detecting potential therapeutic agents [4]. Having an insight into the life cycle of SARS-CoV-2 provides information and helps us identify possible targets for drug development [1]. The SARS-CoV-2 genome encodes 14 open reading frames (ORFs) with a length of around 30 kb. These ORFs encode four structural proteins, nine accessory proteins, and two long polyproteins, pp1a and pp1ab. Two cysteine proteases, the papain-like protease (PLpro) and the main protease (Mpro, also known as 3CLpro), self-catalyse the cleavage of the two polyproteins, pp1a and pp1ab, into 16 non-structural proteins (NSPs) [5,6]. Mpro is a conserved gene in SARS-CoV-2, as well as other highly pathogenic coronavirus, including SARS-CoV-1, MERS-CoV [6-9], Since there are no known human proteases with a similar cleavage specificity and Mpro plays a crucial role in viral replication, it is an ideal target for the development of antivirals. Growing data indicates that 3CLpro, also referred to as the main protease, is essential for the viral replication and has been identified as a major target for the prevention and treatment of infectious diseases caused by coronaviruses, such as COVID-19 [10]. The protease enzyme plays a critical role in viral protein maturation by cleaving the pro-proteins after their translation into the host cell cytosol. As a result of this, the viral proteases are often considered potential drug targets. Mature viral particle assembly may be inhibited by blocking viral protease.

Proteases have been the focus of several antiviral drugs developed to date to combat viral infection [3]. Small molecules have several advantages like favorable oral bioavailability and a rational design [11], besides that they often have low target selectivity, ultimately resulting in side effects. In contrast, despite having a strong affinity and specificity for their target proteins, peptides were frequently overlooked as possible targets for drug development. Compared to proteins, they are smaller and can be produced synthetically using reliable and affordable techniques [12]. So far, more than 11.8 billion vaccine doses have been administered [2,13] Remdesivir, Dexamethasone, Favipiravir, Lopinavir/Ritonavir, Nirmatrelvir/Ritonavir (Main protease inhibitor), and Darunavir have been approved for emergency use to inhibit SARS-CoV-2 infection and replication [14-19]. Additionally, three antivirals—Azvudine, Renmindevir, and Xiannuoxin (a combination of Simnotrelvir and Ritonavir) were authorised by the Chinese National Medical Products Administration [19]. Of them, Remdesivir [20], Molnupiravir [21], Renmindevir [22], and Azvudine [23] is involved in the inhibition of SARS-CoV-2 RdRp. On the other hand, Nirmatrelvir [14], Ensitrelvir [24], and Simnotrelvir [19] inhibits SARS-CoV-2 Mpro. However,

they have several shortcomings as a consequence of the pandemic emergency response, such as inadequate potency, toxicity, or pharmacokinetic (PK) characteristics, such as low oral drug exposure, poor oral bioavailability, and intermediate stability in human liver microsomes [20-22, 14, 25]. Moreover, drug resistance variants against currently approved drugs have already emerged. For example, it has been reported that Mpro variants with E166N/V, M165T, G143S, Q189E, A173V, H172F/Q/Y, or Q192S/T/V mutations are resistant to Nimatrelvir treatment [26-30].

Given a considerable limitation of direct-acting antivirals for COVID-19 and an increasing presence of SARS-CoV-2 variants (B.1.1.529, B.1.617.2, B.1.1.7, B.1.351, A.23.1, B.1.525, B.1.526 and P.1) [31], it remains a strategic priority to develop new drug candidates with minimal side effects and also targeting the new variants. Though a generous number of peptide inhibitors has been developed but it is believed that more peptide inhhibitors still needs to be developed which can more effectively diminish the effect of the disease. Hereby, this work mainly involves the designing of the peptide which binds to the active site of the Mpro and may inhibit its functioning. The main challenge in desginingthe peptide inhibitor for Mpro will be looking for the interacting residues at the interface between Mpro and other biomolecule in the complex form. According to literature survey, Gordon et.al., identified one high-confidence interaction between the main protease(Mpro) and the epigenetic regulator histone deacetylase 2 (HDAC2) [32]. Based on the interacting residues at the interface between the Mpro and HDAC2, a total of 13 peptide sequences were designed. Now based on selective preliminary in-silico analysis which include toxicity, binding site prediction and binding affinity analysis, out of all 13 peptides we screened two peptides (Peptide2 and Peptide4) and were subjected to MD simulation.

In this study, we compared the interaction profile as well as the binding profile of the Mpro with the newly designed peptides. We observed through the MD simulation that both the peptides bind actively to the active site of the Mpro, followed by the binding affinity analysis of the complexes which was found to be indeed high (GB_{TOT} = -72.85 kcal/mol) in case of the Mpro-peptide2 complex in comparison with Mpro-peptide4 complex (GB_{TOT} = -46.36 kcal/mol).

6.3. Materials and Methods:

6.3.1. *Initial structure preparation and molecular docking*

6.3.1.1. Preparation of the receptor (Mpro) and HDAC2.

Our first aim was to find the interaction between the main protease (Mpro) and the Histone deacetylase 2 (HDAC2). In order to carry out the work, the 3D structure of SARS-CoV-2 Main protease was downloaded from the Research Collaboratory for Structural Bioinformatics- Protein Data Bank (RCSB-

PDB) with PDB Id 6Y84 and that of the HDAC2 was downloaded from the same with PDB Id 7ZZO.

6.3.1.2. Preparation of SARS-CoV-2 Mpro-HDAC2 complex

The complex structure (Mpro-HDAC2) was prepared using ClusPro online docking server [33,34] and the 3D structure of the complex is shown in **Figure 6.1.** The ClusPro server (https://cluspro.org) is a widely used tool for protein-protein docking. The server provides a simple home page for basic use, requiring only two files in Protein Data Bank (PDB) format. The orientation of the model complex structure (Mpro-HDAC2) obtained from Cluspro was checked with the modelled structure obtained from HDOCK (another docking server) [35,36]. It was observed that the RMSD difference between both the structures was found to be 0.004 Å (**Figure 6.2**). The complex structure obtained from the ClusPro server was then validated using VERIFY-3D [37], ERRAT [38] and PROCHECK from PDBsum server [39]. The results obtained from the VERIFY3D shows that 88.11% of the residues have averaged 3D-1D score >= 0.1. ERRAT results shows an overall quality factor of 93.72% and the allowed and disallowed regions obtained from the Ramachandran plot using PROCHECK is summarized in **Figure 6.3**. Therefore, we proceeded our study with the docked structure obtained from the ClusPro.

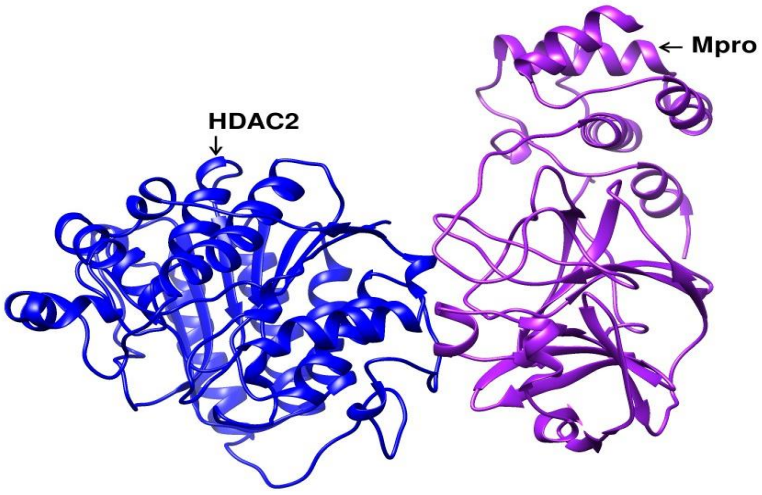

Figure 6.1. *The 3-D structure of SARS-CoV-2 Main protease (Mpro) bound with Histone deacetylase 2 (HDAC2).*

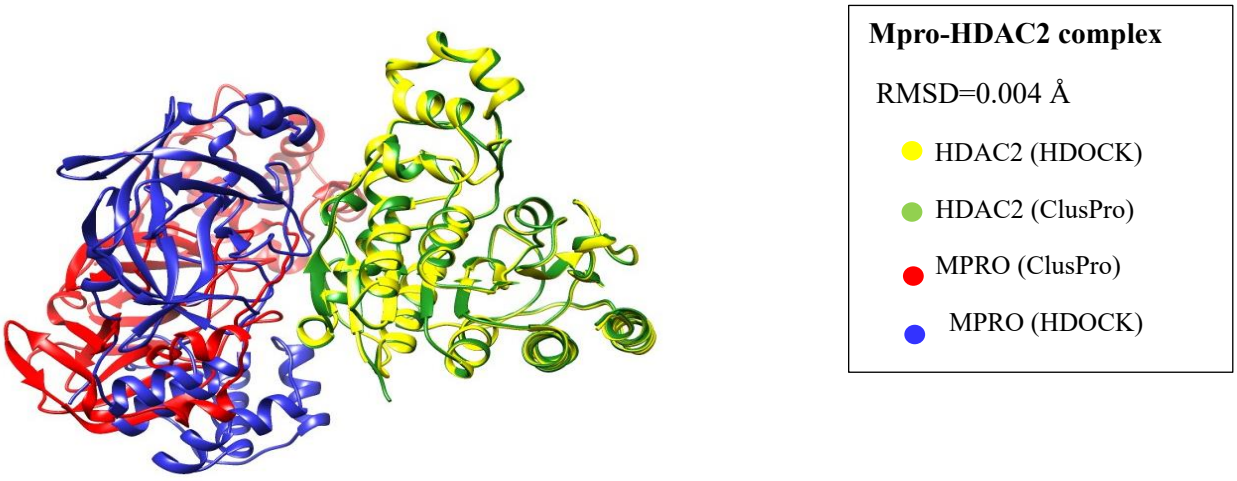

Figure 6.2. *Superimposition of the Mpro-HDAC2 complex obtained from Cluspro and HDOCK. The box at the right shows the significance of different colors along with the RMSD values.*

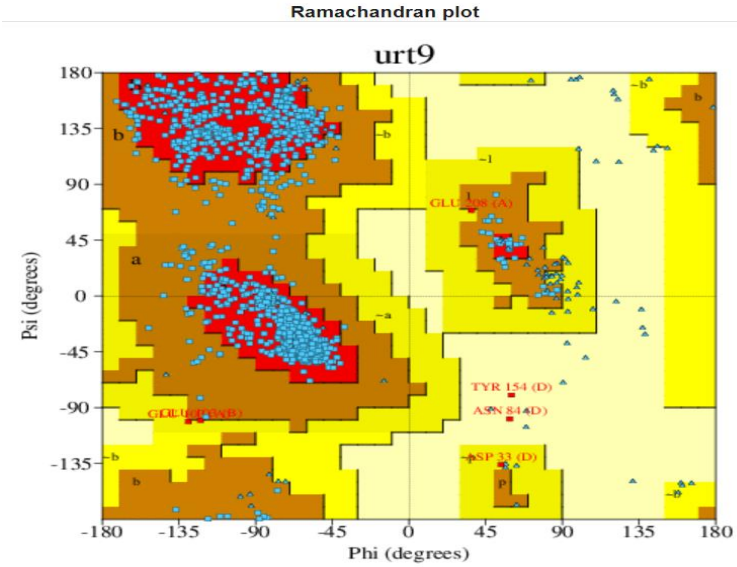

	No. of residues	%-tage
	------	------
Most favoured regions[A,B,L]	1074	88.2%*
Additional allowed regions [a,b,l,p]	137	11.3%

Figure 6.3. *Ramachandran plot obtained from PROCHECK for the validation of the Mpro-HDAC2 complex structure*

6.3.2. Determination of the protein-protein interface interactions of the (Mpro-HDAC2) complex

Proteins can interact multivalently with a myriad of various biomolecules, including other proteins and nucleic acids. The strength and physicochemical character of intermolecular contacts between these complex systems is a driving force of signalling or regulatory processes, while the identification of these contacts in the available 3D structures is essential for biomedical and biotechnological applications. To

obtain the interacting residue statistics for the Mpro-HDAC2 complex, we submitted the docked structure to the Mapiya server. Mapiya web [40] service offers a highly customized analysis of the molecular interactions in biological systems using contact maps, molecular visualization, and various structure- and sequence-based analyses.

Results showed a total of 426 interactions between the Mpro and the HDAC2 which includes the electrostatic, dipole-dipole, hydrogen bond, π-π stacking, dipole-π stacking etc. Here we will be considering only the electrostatic (ELE) interaction between the Mpro and the HDAC2. And we found a total of 109 ELE interaction between them. Among all 109 ELE contacts we screened out only those with distance less than or equal to 5Å.

There were 28 ELE contacts with distance less than or equal to 5Å listed in **Table 6.1.**

Table 6.1. *Electrostatic contacts between Mpro and HDAC2 with distance less than or equal to 5 Å.*

Sl.No.	Residues from Mpro (chain A)	Residues from HDAC2 (chain B)	Distance (Å)
1	ASN:51	ASP:337	4.684
2	ASN:84	GLU:340	4.873
3	CYS:85	GLU:340	3.413
4	ASN:133	ARG:275	2.849
5	THR:169	GLN:31	2.831
6	THR:169	TYR:28	3.446
7	GLN:192	TYR:341	2.755
8	GLN:192	HIS:38	3.484
9	GLN:192	TYR:338	4.594
10	THR:196	ARG:275	3.404
11	THR:196	TYR:308	3.709
12	THR:196	LYS:36	4.986
13	THR:198	ARG:275	3.537
14	ASN:228	GLN:358	2.904
15	ASN:228	ARG:234	3.831
16	ASN:228	ASP:235	3.928
17	ASN:231	ASP:235	3.574
18	ASN:231	GLN:358	3.781
19	ASN:231	CYS:278	4.199
20	ASN:231	LYS:205	4.409
21	MET:235	LYS:205	3.282
22	MET:235	LYS:278	3.325
23	MET:235	TYR:209	3.356
24	MET:235	ASP:235	3.639
25	THR:243	MET:355	4.21
26	GLN:244	THR:356	4.705
27	ASP:245	ASN:354	2.825
28	GLN:273	GLU:208	2.923

6.3.3. Designing of peptides

Based on the interacting residues of the HDAC2, we designed the peptides taking into consideration an optimal length of 16 amino acids (https://www.abcam.com/protocols/tips-for-designing-a-good-peptide-immunogen). Out of the 28 residues of the HDAC2, selecting 16 residues at a time and based on the sliding method (sliding one amino acid at a time) we got 13 peptide sequences as shown in **Figure 6.4.**

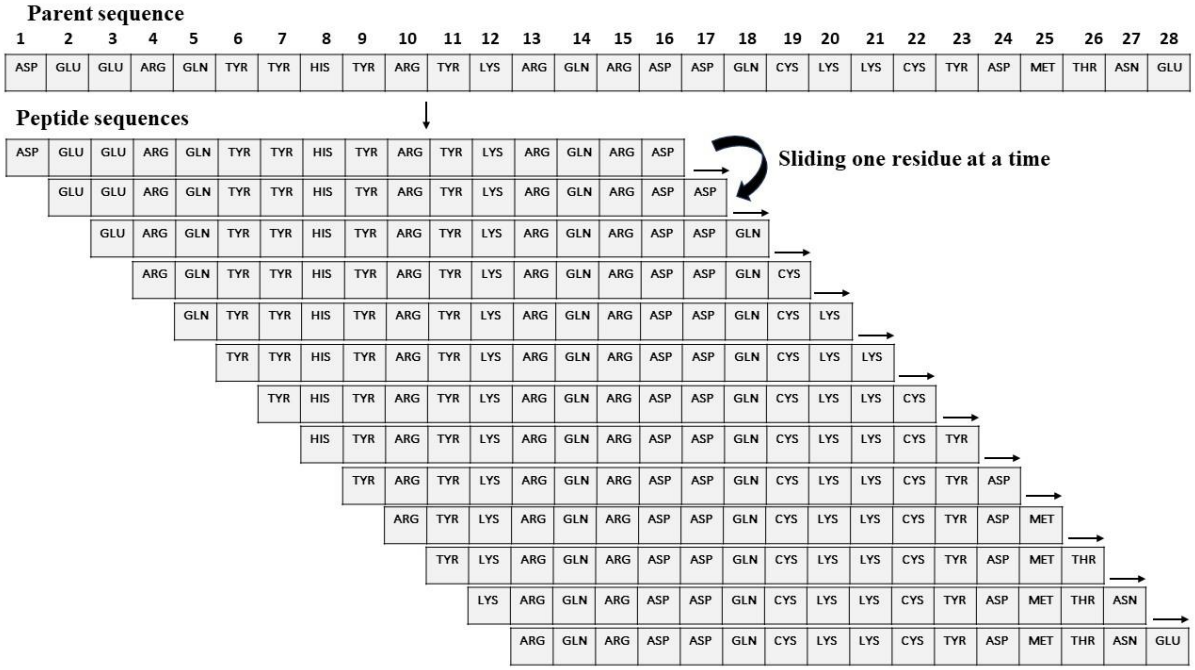

Figure 6.4. *Designing of the peptides from the parent sequence.*

Figure 6.4 shows the 13 peptide sequences generated from the parent sequence and the same has been tabulated in **Table 6.2.** Out of those 13 peptide sequences we screened out screened top 2 peptide sequences based on some preliminary in-silico analysis.

Table 6.2. *Showing the sequences of all 13 designed peptides*

Peptide	Sequence
Peptide 1	ASP, GLU, GLU, ARG, GLN, TYR, TYR, HIS, TYR, ARG, TYR, LYS, ARG, GLN, ARG, ASP
Peptide 2	GLU, GLU, ARG, GLN, TYR, TYR, HIS, TYR, ARG, TYR, LYS, ARG, GLN, ARG, ASP, ASP
Peptide 3	GLU, ARG, GLN, TYR, TYR, HIS, TYR, ARG, TYR, LYS, ARG, GLN, ARG, ASP, ASP, GLN
Peptide 4	ARG, GLN, TYR, TYR, HIS, TYR, ARG, TYR, LYS, ARG, GLN, ARG, ASP, ASP, GLN, CYS
Peptide 5	GLN, TYR, TYR, HIS, TYR, ARG, TYR, LYS, ARG, GLN, ARG, ASP, ASP, GLN, CYS, LYS

Peptide 6	TYR, TYR, HIS, TYR, ARG, TYR, LYS, ARG, GLN, ARG, ASP, ASP, GLN, CYS, LYS, LYS
Peptide 7	TYR, HIS, TYR, ARG, TYR, LYS, ARG, GLN, ARG, ASP, ASP, GLN, CYS, LYS, LYS, CYS
Peptide 8	HIS, TYR, ARG, TYR, LYS, ARG, GLN, ARG, ASP, ASP, GLN, CYS, LYS, LYS, CYS, TYR
Peptide 9	TYR, ARG, TYR, LYS, ARG, GLN, ARG, ASP, ASP, GLN, CYS, LYS, LYS, CYS, TYR, ASP
Peptide 10	ARG, TYR, LYS, ARG, GLN, ARG, ASP, ASP, GLN, CYS, LYS, LYS, CYS, TYR, ASP, MET
Peptide 11	TYR, LYS, ARG, GLN, ARG, ASP, ASP, GLN, CYS, LYS, LYS, CYS, TYR, ASP, MET, THR
Peptide 12	LYS, ARG, GLN, ARG, ASP, ASP, GLN, CYS, LYS, LYS, CYS, TYR, ASP, MET, THR, ASN
Peptide 13	ARG, GLN, ARG, ASP, ASP, GLN, CYS, LYS, LYS, CYS, TYR, ASP, MET, THR, ASN, GLU

6.3.4. Preparation of the peptide-Mpro complexes

In order to do the screening of the peptides and to perform the further analysis, we have constructed the Mpro-peptide complexes. We have docked the Mpro with the individual peptides using the CABS-DOCK online server [41, 42]. The CABS-dock web server provides an interface for modelling protein-peptide interactions using a highly efficient protocol for the flexible docking of peptides to proteins. While many other docking algorithms require a predetermined binding site location, CABS-dock does not. Given a protein receptor structure and a peptide sequence (and starting from random conformations and positions of the peptide), CABS-dock performs simulation search for the binding site allowing for full flexibility of the peptide and small fluctuations of the receptor backbone. Furthermore, the advanced option "Mark flexible regions" allows you to fully customize a specific segment of a protein receptor structure. Looking at all those advantages of CABS-dock we ended up selecting this server.

The docked complexes obtained from CABS-dock for all the 13 peptides are shown in **Figure 6.5**.

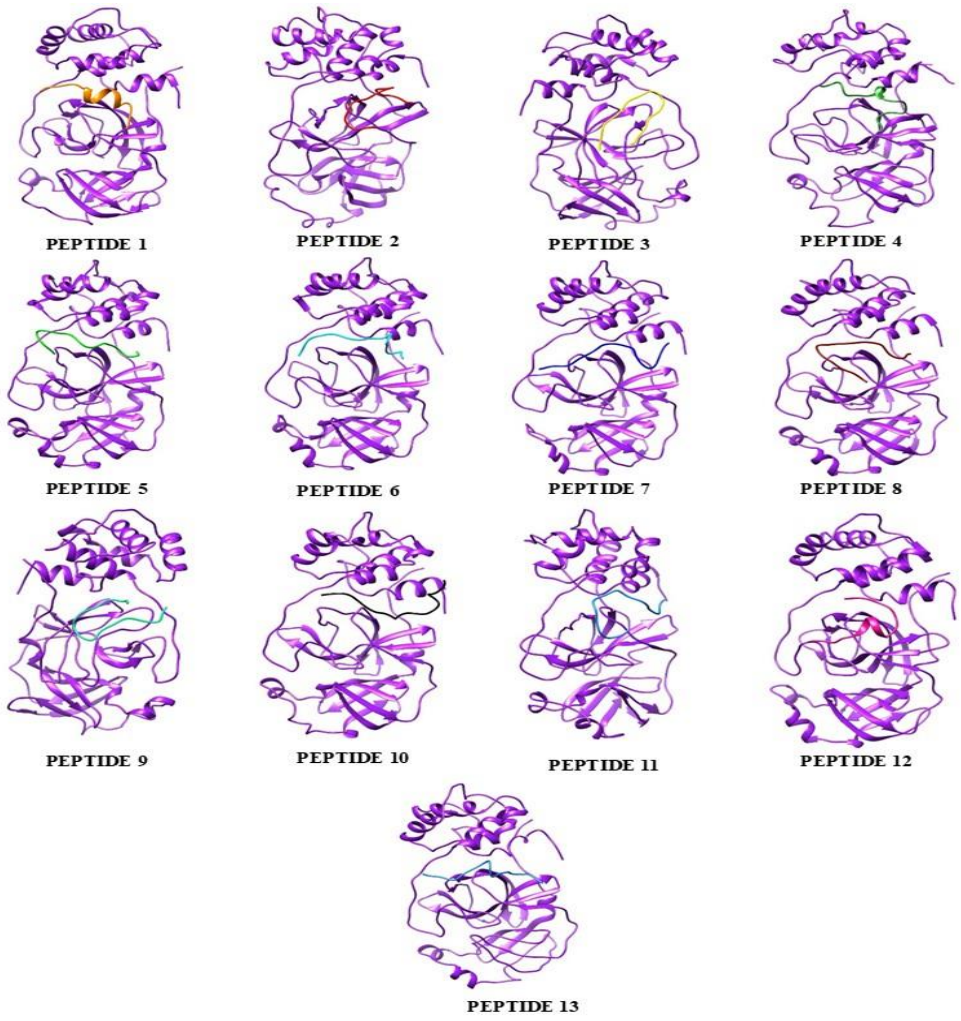

Figure 6.5. *The docked complexes for all the 13 peptides (shown in different colors) and Mpro (purple)*

6.3.5. Screening of peptides

6.3.5.1. Toxicity

The first and foremost thing after designing the peptides is analysing whether the peptide is toxic or non-toxic. If the peptide is toxic there is no point of considering that peptide to design inhibitor and perform the further analysis. We analysed the toxicity of all the 13 peptides using a web-server, ToxIBTL [43], a novel deep learning framework by exploiting the information bottleneck principle and transfer learning to predict the toxicity of peptides as well as proteins.

Based on the toxicity analysis we found that out of the 13 peptides, 8 peptides were non-toxic and the list is shown in **Table 6.3**.

Table 6.3. *The toxicity analysis of all 13 peptides using ToxIBTL*

Peptide	Toxicity
Peptide 1	Non-toxic
Peptide 2	Non-toxic
Peptide 3	Non-toxic
Peptide 4	Non-toxic
Peptide 5	Non-toxic
Peptide 6	Non-toxic
Peptide 7	Non-toxic
Peptide 8	Toxic
Peptide 9	Non-toxic
Peptide 10	Toxic
Peptide 11	Toxic
Peptide 12	Toxic
Peptide 13	Toxic

Now we will be considering those 8 non-toxic peptides (peptide 1, peptide 2, peptide 3, peptide 4, peptide 5, peptide 6, peptide 7, peptide 9) for the further analysis.

6.3.5.2. Binding affinity between the Mpro and Peptides

We analysed the binding affinity between the Mpro and the individual peptides using the PRODIGY web server [44]. PRODIGY (PROtein binDIng enerGY prediction) is a collection of web services focused on the prediction of binding affinity in biological complexes as well as the identification of biological interfaces from crystallographic one. **Table 6.4** shows the ΔG values for the 8 peptides.

Table 6.4*. Binding free energy (ΔG) values between the Mpro and peptides.*

Peptide	ΔG (kcal/mol)
Peptide 1	-9.6
Peptide 2	**-14.0**
Peptide 3	-11.3
Peptide 4	**-12.6**
Peptide 5	-10.9
Peptide 6	-10.4
Peptide 7	-10.6
Peptide 9	-11.8

From the binding affinity analysis, we found that the peptide 2 and peptide 4 shows the highest binding affinity with the Mpro suggesting a strong interaction between the peptide and the Mpro.

Eberle et al., [45] in their study have designed peptides against Mpro which we considered as the positive control for our study. We compared the binding affinity of those control peptides (3CVL-2, 3CVL-4 and 3CVL-7) with our designed peptides with Mpro using Prodigy server and results are shown in **Table 6.5.** We found that the binding affinity was more in case of our designed peptides as compared to the positive controls.

Table 6.5. *Binding free energy (ΔG) values between the Mpro and positive control peptides (3CVL-2, 3CVL-4, 3CVL-7)*

Peptides	ΔG (kcal/mol)
Peptide 2	-14.0
Peptide 4	-12.6
3CVL-2	-12.1
3CVL-4	-11.7
3CVL-7	-10.3

6.3.5.3. Interaction study between Mpro and Peptides

In order to inhibit the Mpro, the designed peptides should bind to the active site of the Mpro. We therefore performed the protein-peptide interaction study to check whether those 8 screened peptides bind to the active site of the Mpro or not.

We performed the protein-peptide interaction study using the PDBsum server [39]. PDBsum is a web server providing structural information on the entries in the Protein Data Bank (PDB). The analyses are primarily image-based and include protein secondary structure, protein-ligand and protein-DNA interactions, PROCHECK analyses of structural quality, and many others.

Interestingly, among the 8 peptides, we found that the two peptides (peptide 2 and peptide 4) that was found to have the highest binding affinity also has the highest number of interactions with the Mpro and that too with the active site of the Mpro**.** Additionally, supplementary **Table 6.6.A, 6.6.B, 6.6.C and 6.7.A, 6.7.B, 6.7.C** respectively, lists the atom-atom interactions (hydrogen bonds, non-bonded contacts, and salt bridges) across the protein-peptide interface in Mpro (chain A)- Peptide (Chain B) exclusively for the two complexes (Mpro-Peptide2 and Mpro-Peptide4) obtained from PDBsum server.

Table 6.6.A: *List of atom-atom interactions (Hydrogen bonds) across protein-peptide interface in Mpro (Chain A) and Peptide2 (Chain B) complex from PDBsum server*

Mpro (Chain A)						Hydrogen bonds	Peptide2 (Chain B)					
Sl.no	Atom no.	Atom name	Res name	Res no.	Chain		Atom no.	Atom name	Res name	Res no.	Chain	Distance
1	840	NE2	GLN	107	A	<-->	2397	OH	TYR	5	B	2.9
2	840	NE2	GLN	107	A	<-->	2504	O	ASP	15	B	2.86
3	984	OE1	GLN	127	A	<-->	2385	NE2	GLN	4	B	3.05
4	1158	ND2	ASN	151	A	<-->	2387	O	GLN	4	B	2.94
5	1213	OG	SER	158	A	<-->	2364	OE1	GLU	2	B	3.06
6	1913	O	ASP	245	A	<-->	2409	OH	TYR	6	B	2.58
7	1910	OD1	ASP	245	A	<-->	2409	OH	TYR	6	B	3.06
8	2347	O	THR	304	A	<-->	2376	NH2	ARG	3	B	3.26

Table 6.6.B. *List of atom-atom interactions (Non-bonded) across protein-peptide interface in Mpro (Chain A) and Peptide2 (Chain B) complex from PDBsum server*

Mpro (Chain A)						Non-bonded	Peptide2 (Chain B)					
Sl.no.	Atom no.	Atom name	Res name	Res no.	Chain		Atom no.	Atom name	Res name	Res no.	Chain	Distance
1	812	CG2	VAL	104	A	<-->	2362	CG	GLU	2	B	3.82
2	812	CG2	VAL	104	A	<-->	2363	CD	GLU	2	B	3.74
3	812	CG2	VAL	104	A	<-->	2365	OE2	GLU	2	B	3.19
4	824	C	ARG	105	A	<-->	2512	O	ASP	16	B	3.73
5	825	O	ARG	105	A	<-->	2397	OH	TYR	5	B	3.88
6	825	O	ARG	105	A	<-->	2512	O	ASP	16	B	2.83
7	817	CB	ARG	105	A	<-->	2512	O	ASP	16	B	3.59
8	818	CG	ARG	105	A	<-->	2491	NE	ARG	14	B	3.55
9	818	CG	ARG	105	A	<-->	2492	CZ	ARG	14	B	3.59
10	818	CG	ARG	105	A	<-->	2494	NH2	ARG	14	B	2.87
11	819	CD	ARG	105	A	<-->	2491	NE	ARG	14	B	3.8
12	819	CD	ARG	105	A	<-->	2494	NH2	ARG	14	B	3.59
13	826	N	ILE	106	A	<-->	2494	NH2	ARG	14	B	3.49
14	832	C	ILE	106	A	<-->	2494	NH2	ARG	14	B	3.81
15	833	O	ILE	106	A	<-->	2491	NE	ARG	14	B	3.38
16	833	O	ILE	106	A	<-->	2492	CZ	ARG	14	B	3.13
17	833	O	ILE	106	A	<-->	2494	NH2	ARG	14	B	2.84
18	835	CA	GLN	107	A	<-->	2488	CB	ARG	14	B	3.83
19	836	CB	GLN	107	A	<-->	2456	O	TYR	10	B	3.89
20	837	CG	GLN	107	A	<-->	2456	O	TYR	10	B	2.87
21	837	CG	GLN	107	A	<-->	2496	O	ARG	14	B	3.7
22	837	CG	GLN	107	A	<-->	2488	CB	ARG	14	B	3.82
23	838	CD	GLN	107	A	<-->	2397	OH	TYR	5	B	3.23

24	838	CD	GLN	107	A	<-->	2456	O	TYR	10	B	3.47
25	838	CD	GLN	107	A	<-->	2504	O	ASP	15	B	3.88
26	839	OE1	GLN	107	A	<-->	2394	CE1	TYR	5	B	3.86
27	839	OE1	GLN	107	A	<-->	2395	CE2	TYR	5	B	3.36
28	839	OE1	GLN	107	A	<-->	2396	CZ	TYR	5	B	3.08
29	839	OE1	GLN	107	A	<-->	2397	OH	TYR	5	B	2.82
30	840	NE2	GLN	107	A	<-->	2397	OH	TYR	5	B	2.9
31	840	NE2	GLN	107	A	<-->	2503	C	ASP	15	B	3.44
32	840	NE2	GLN	107	A	<-->	2504	O	ASP	15	B	2.86
33	840	NE2	GLN	107	A	<-->	2505	N	ASP	16	B	3.53
34	840	NE2	GLN	107	A	<-->	2506	CA	ASP	16	B	2.97
35	840	NE2	GLN	107	A	<-->	2511	C	ASP	16	B	3.79
36	840	NE2	GLN	107	A	<-->	2512	O	ASP	16	B	3.81
37	846	CB	PRO	108	A	<-->	2473	NH1	ARG	12	B	3.15
38	847	CG	PRO	108	A	<-->	2475	C	ARG	12	B	3.88
39	847	CG	PRO	108	A	<-->	2476	O	ARG	12	B	2.9
40	847	CG	PRO	108	A	<-->	2479	CB	GLN	13	B	3.48
41	847	CG	PRO	108	A	<-->	2489	CG	ARG	14	B	3.62
42	845	CD	PRO	108	A	<-->	2476	O	ARG	12	B	2.8
43	845	CD	PRO	108	A	<-->	2488	CB	ARG	14	B	3.49
44	845	CD	PRO	108	A	<-->	2489	CG	ARG	14	B	3.04
45	857	CG	GLN	110	A	<-->	2389	CA	TYR	5	B	3.76
46	857	CG	GLN	110	A	<-->	2398	C	TYR	5	B	3.52
47	857	CG	GLN	110	A	<-->	2399	O	TYR	5	B	3.58
48	860	NE2	GLN	110	A	<-->	2402	CB	TYR	6	B	3.76
49	860	NE2	GLN	110	A	<-->	2405	CD2	TYR	6	B	3.87
50	860	NE2	GLN	110	A	<-->	2447	CB	TYR	10	B	3.24
51	868	C	THR	111	A	<-->	2387	O	GLN	4	B	3.9
52	869	O	THR	111	A	<-->	2386	C	GLN	4	B	3.6
53	869	O	THR	111	A	<-->	2387	O	GLN	4	B	2.71
54	869	O	THR	111	A	<-->	2381	CB	GLN	4	B	3.37
55	884	OG	SER	113	A	<-->	2384	OE1	GLN	4	B	3.78
56	983	CD	GLN	127	A	<-->	2385	NE2	GLN	4	B	3.84
57	984	OE1	GLN	127	A	<-->	2383	CD	GLN	4	B	3.81
58	984	OE1	GLN	127	A	<-->	2385	NE2	GLN	4	B	3.05
59	1019	CA	PRO	132	A	<-->	2473	NH1	ARG	12	B	3.59
60	1021	CB	PRO	132	A	<-->	2472	CZ	ARG	12	B	3.55
61	1021	CB	PRO	132	A	<-->	2473	NH1	ARG	12	B	3.14
62	1021	CB	PRO	132	A	<-->	2474	NH2	ARG	12	B	3.08
63	1038	CD2	PHE	134	A	<-->	2493	NH1	ARG	14	B	3.01
64	1039	CE1	PHE	134	A	<-->	2482	OE1	GLN	13	B	3.65
65	1040	CE2	PHE	134	A	<-->	2489	CG	ARG	14	B	3.12
66	1040	CE2	PHE	134	A	<-->	2490	CD	ARG	14	B	3.25
67	1040	CE2	PHE	134	A	<-->	2491	NE	ARG	14	B	3.8
68	1040	CE2	PHE	134	A	<-->	2492	CZ	ARG	14	B	3.64

69	1040	CE2	PHE	134	A	<-->	2493	NH1	ARG	14	B	2.94
70	1041	CZ	PHE	134	A	<-->	2485	O	GLN	13	B	3.37
71	1041	CZ	PHE	134	A	<-->	2489	CG	ARG	14	B	3.08
72	1041	CZ	PHE	134	A	<-->	2490	CD	ARG	14	B	3.32
73	1041	CZ	PHE	134	A	<-->	2493	NH1	ARG	14	B	3.8
74	1156	CG	ASN	151	A	<-->	2387	O	GLN	4	B	3.25
75	1157	OD1	ASN	151	A	<-->	2387	O	GLN	4	B	3.3
76	1157	OD1	ASN	151	A	<-->	2381	CB	GLN	4	B	3.25
77	1157	OD1	ASN	151	A	<-->	2384	OE1	GLN	4	B	3.31
78	1158	ND2	ASN	151	A	<-->	2387	O	GLN	4	B	2.94
79	1168	O	ILE	152	A	<-->	2370	CB	ARG	3	B	3.8
80	1168	O	ILE	152	A	<-->	2373	NE	ARG	3	B	3.43
81	1170	CA	ASP	153	A	<-->	2373	NE	ARG	3	B	3.75
82	1173	OD1	ASP	153	A	<-->	2371	CG	ARG	3	B	3.42
83	1173	OD1	ASP	153	A	<-->	2372	CD	ARG	3	B	3.77
84	1173	OD1	ASP	153	A	<-->	2373	NE	ARG	3	B	3.68
85	1174	OD2	ASP	153	A	<-->	2350	N	GLU	1	B	3.83
86	1174	OD2	ASP	153	A	<-->	2357	C	GLU	1	B	3.82
87	1174	OD2	ASP	153	A	<-->	2358	O	GLU	1	B	3.18
88	1212	CB	SER	158	A	<-->	2363	CD	GLU	2	B	2.93
89	1212	CB	SER	158	A	<-->	2364	OE1	GLU	2	B	2.82
90	1212	CB	SER	158	A	<-->	2365	OE2	GLU	2	B	2.91
91	1213	OG	SER	158	A	<-->	2363	CD	GLU	2	B	3.48
92	1213	OG	SER	158	A	<-->	2364	OE1	GLU	2	B	3.06
93	1353	OD1	ASP	176	A	<-->	2494	NH2	ARG	14	B	3.57
94	1354	OD2	ASP	176	A	<-->	2494	NH2	ARG	14	B	3.55
95	1398	CA	TYR	182	A	<-->	2493	NH1	ARG	14	B	3.58
96	1399	CB	TYR	182	A	<-->	2493	NH1	ARG	14	B	3.56
97	1400	CG	TYR	182	A	<-->	2493	NH1	ARG	14	B	3.66
98	1402	CD2	TYR	182	A	<-->	2492	CZ	ARG	14	B	3.51
99	1402	CD2	TYR	182	A	<-->	2493	NH1	ARG	14	B	3.02
100	1402	CD2	TYR	182	A	<-->	2494	NH2	ARG	14	B	3.15
101	1404	CE2	TYR	182	A	<-->	2494	NH2	ARG	14	B	3.2
102	1871	OE1	GLU	240	A	<-->	2454	OH	TYR	10	B	3.77
103	1871	OE1	GLU	240	A	<-->	2470	CD	ARG	12	B	3.85
104	1892	CB	THR	243	A	<-->	2454	OH	TYR	10	B	3.88
105	1894	CG2	THR	243	A	<-->	2451	CE1	TYR	10	B	3.89
106	1894	CG2	THR	243	A	<-->	2454	OH	TYR	10	B	3.15
107	1907	CA	ASP	245	A	<-->	2409	OH	TYR	6	B	3.82
108	1912	C	ASP	245	A	<-->	2409	OH	TYR	6	B	2.88
109	1913	O	ASP	245	A	<-->	2409	OH	TYR	6	B	2.58
110	1908	CB	ASP	245	A	<-->	2409	OH	TYR	6	B	3.71
111	1908	CB	ASP	245	A	<-->	2451	CE1	TYR	10	B	3.71
112	1909	CG	ASP	245	A	<-->	2409	OH	TYR	6	B	3.39
113	1910	OD1	ASP	245	A	<-->	2406	CE1	TYR	6	B	3.82

114	1910	OD1	ASP	245	A	<-->	2408	CZ	TYR	6	B	3.79
115	1910	OD1	ASP	245	A	<-->	2409	OH	TYR	6	B	3.06
116	1911	OD2	ASP	245	A	<-->	2449	CD1	TYR	10	B	3.77
117	1914	N	HIS	246	A	<-->	2409	OH	TYR	6	B	3.16
118	1915	CA	HIS	246	A	<-->	2409	OH	TYR	6	B	3.2
119	1946	O	ILE	249	A	<-->	2416	CB	HIS	7	B	3.55
120	1941	CB	ILE	249	A	<-->	2406	CE1	TYR	6	B	3.14
121	1941	CB	ILE	249	A	<-->	2408	CZ	TYR	6	B	3.07
122	1941	CB	ILE	249	A	<-->	2409	OH	TYR	6	B	2.95
123	1942	CG1	ILE	249	A	<-->	2404	CD1	TYR	6	B	3.56
124	1942	CG1	ILE	249	A	<-->	2406	CE1	TYR	6	B	3.2
125	1942	CG1	ILE	249	A	<-->	2408	CZ	TYR	6	B	3.42
126	1942	CG1	ILE	249	A	<-->	2409	OH	TYR	6	B	3.88
127	1942	CG1	ILE	249	A	<-->	2412	N	HIS	7	B	3.19
128	1942	CG1	ILE	249	A	<-->	2413	CA	HIS	7	B	3.61
129	1942	CG1	ILE	249	A	<-->	2416	CB	HIS	7	B	2.95
130	1943	CG2	ILE	249	A	<-->	2408	CZ	TYR	6	B	3.46
131	1943	CG2	ILE	249	A	<-->	2409	OH	TYR	6	B	3
132	1944	CD1	ILE	249	A	<-->	2401	CA	TYR	6	B	3.79
133	1944	CD1	ILE	249	A	<-->	2410	C	TYR	6	B	3.8
134	1944	CD1	ILE	249	A	<-->	2403	CG	TYR	6	B	2.99
135	1944	CD1	ILE	249	A	<-->	2404	CD1	TYR	6	B	3.01
136	1944	CD1	ILE	249	A	<-->	2405	CD2	TYR	6	B	2.96
137	1944	CD1	ILE	249	A	<-->	2406	CE1	TYR	6	B	2.99
138	1944	CD1	ILE	249	A	<-->	2407	CE2	TYR	6	B	2.94
139	1944	CD1	ILE	249	A	<-->	2408	CZ	TYR	6	B	2.95
140	1944	CD1	ILE	249	A	<-->	2409	OH	TYR	6	B	3.8
141	1944	CD1	ILE	249	A	<-->	2412	N	HIS	7	B	2.93
142	1944	CD1	ILE	249	A	<-->	2416	CB	HIS	7	B	3.82
143	2253	CB	THR	292	A	<-->	2399	O	TYR	5	B	3.48
144	2254	OG1	THR	292	A	<-->	2399	O	TYR	5	B	3.36
145	2255	CG2	THR	292	A	<-->	2398	C	TYR	5	B	3.83
146	2255	CG2	THR	292	A	<-->	2399	O	TYR	5	B	2.75
147	2264	O	PRO	293	A	<-->	2410	C	TYR	6	B	3.8
148	2264	O	PRO	293	A	<-->	2412	N	HIS	7	B	3.55
149	2267	CB	PHE	294	A	<-->	2378	O	ARG	3	B	3.06
150	2268	CG	PHE	294	A	<-->	2377	C	ARG	3	B	3.67
151	2268	CG	PHE	294	A	<-->	2378	O	ARG	3	B	2.74
152	2269	CD1	PHE	294	A	<-->	2369	CA	ARG	3	B	3.62
153	2269	CD1	PHE	294	A	<-->	2377	C	ARG	3	B	3.26
154	2269	CD1	PHE	294	A	<-->	2378	O	ARG	3	B	2.73
155	2269	CD1	PHE	294	A	<-->	2370	CB	ARG	3	B	3.62
156	2270	CD2	PHE	294	A	<-->	2378	O	ARG	3	B	3.45
157	2271	CE1	PHE	294	A	<-->	2369	CA	ARG	3	B	3.36
158	2271	CE1	PHE	294	A	<-->	2377	C	ARG	3	B	3.6

159	2271	CE1	PHE	294	A	<-->	2378	O	ARG	3	B	3.42
160	2271	CE1	PHE	294	A	<-->	2370	CB	ARG	3	B	3.04
161	2271	CE1	PHE	294	A	<-->	2371	CG	ARG	3	B	3.06
162	2271	CE1	PHE	294	A	<-->	2372	CD	ARG	3	B	3.13
163	2273	CZ	PHE	294	A	<-->	2369	CA	ARG	3	B	3.74
164	2273	CZ	PHE	294	A	<-->	2370	CB	ARG	3	B	3.66
165	2273	CZ	PHE	294	A	<-->	2371	CG	ARG	3	B	3.23
166	2273	CZ	PHE	294	A	<-->	2372	CD	ARG	3	B	3.44
167	2279	CG	ASP	295	A	<-->	2381	CB	GLN	4	B	3.65
168	2279	CG	ASP	295	A	<-->	2382	CG	GLN	4	B	3.61
169	2279	CG	ASP	295	A	<-->	2385	NE2	GLN	4	B	3.88
170	2280	OD1	ASP	295	A	<-->	2380	CA	GLN	4	B	2.96
171	2280	OD1	ASP	295	A	<-->	2381	CB	GLN	4	B	2.89
172	2280	OD1	ASP	295	A	<-->	2382	CG	GLN	4	B	2.74
173	2280	OD1	ASP	295	A	<-->	2383	CD	GLN	4	B	3.54
174	2280	OD1	ASP	295	A	<-->	2385	NE2	GLN	4	B	3.66
175	2281	OD2	ASP	295	A	<-->	2381	CB	GLN	4	B	3.64
176	2281	OD2	ASP	295	A	<-->	2382	CG	GLN	4	B	3.89
177	2336	CB	VAL	303	A	<-->	2375	NH1	ARG	3	B	3.24
178	2337	CG1	VAL	303	A	<-->	2375	NH1	ARG	3	B	3.74
179	2338	CG2	VAL	303	A	<-->	2374	CZ	ARG	3	B	3.81
180	2338	CG2	VAL	303	A	<-->	2375	NH1	ARG	3	B	3.21
181	2347	O	THR	304	A	<-->	2376	NH2	ARG	3	B	3.26

Table 6.6.C. *List of atom-atom interactions (Salt Bridge) across protein-peptide interface in Mpro (Chain A) and Peptide2 (Chain B) complex from PDBsum server*

Mpro (Chain A)						Salt Bridge	Peptide2 (Chain B)					
Sl.no.	Atom no.	Atom name	Res name	Res no.	Chain		Atom no.	Atom name	Res name	Res no.	Chain	Distance
1	1173	OD1	ASP	153	A	<-->	2373	NE	ARG	3	B	3.68
2	1354	OD2	ASP	176	A	<-->	2494	NH2	ARG	14	B	3.55

Table 6.7.A: *List of atom-atom interactions (Hydrogen bonds) across protein-peptide interface in Mpro (Chain A) and Peptide4 (Chain B) complex from PDBsum server*

Mpro (Chain A)						Hydrogen bonds	Peptide4 (Chain B)					
Sl.no.	Atom no.	Atom name	Res name	Res no.	Chain		Atom no.	Atom name	Res name	Res no.	Chain	Distance
1	859	OE1	GLN	110	A	<-->	2421	NE	ARG	7	B	2.69
2	859	OE1	GLN	110	A	<-->	2424	NH2	ARG	7	B	3.26
3	869	O	THR	111	A	<-->	2424	NH2	ARG	7	B	2.81
4	1173	OD1	ASP	153	A	<-->	2475	NH1	ARG	12	B	2.81
5	1881	O	PRO	241	A	<-->	2379	OH	TYR	3	B	2.56

Table 6.7.B: *List of atom-atom interactions (Non-bonded) across protein-peptide interface in Mpro (Chain A) and Peptide4 (Chain B) complex from PDBsum server*

Mpro (Chain A)						Non-bonded	Peptide4 (Chain B)					
Sl.no	Atom no.	Atom name	Res name	Res no.	Chain		Atom No.	Atom name	Res name	Res no.	Chain	Distance
1	807	O	PHE	103	A	<-->	2503	O	GLN	15	B	3.68
2	804	CE2	PHE	103	A	<-->	2505	CA	CYS	16	B	3.65
3	809	CA	VAL	104	A	<-->	2503	O	GLN	15	B	3.52
4	810	CB	VAL	104	A	<-->	2489	CB	ASP	14	B	3.46
5	810	CB	VAL	104	A	<-->	2492	OD2	ASP	14	B	3.58
6	811	CG1	VAL	104	A	<-->	2489	CB	ASP	14	B	2.94
7	811	CG1	VAL	104	A	<-->	2490	CG	ASP	14	B	3.48
8	811	CG1	VAL	104	A	<-->	2492	OD2	ASP	14	B	3.44
9	811	CG1	VAL	104	A	<-->	2495	N	GLN	15	B	3.64
10	811	CG1	VAL	104	A	<-->	2503	O	GLN	15	B	3.75
11	812	CG2	VAL	104	A	<-->	2489	CB	ASP	14	B	2.94
12	812	CG2	VAL	104	A	<-->	2490	CG	ASP	14	B	3.44
13	812	CG2	VAL	104	A	<-->	2492	OD2	ASP	14	B	3.01
14	815	N	ARG	105	A	<-->	2503	O	GLN	15	B	3.64
15	825	O	ARG	105	A	<-->	2497	CB	GLN	15	B	3.4
16	836	CB	GLN	107	A	<-->	2396	ND1	HIS	5	B	3.27
17	836	CB	GLN	107	A	<-->	2401	CE1	HIS	5	B	3.71
18	837	CG	GLN	107	A	<-->	2398	CB	HIS	5	B	3.7
19	837	CG	GLN	107	A	<-->	2397	CG	HIS	5	B	3.71
20	837	CG	GLN	107	A	<-->	2396	ND1	HIS	5	B	3.48
21	856	CB	GLN	110	A	<-->	2424	NH2	ARG	7	B	3.73
22	858	CD	GLN	110	A	<-->	2421	NE	ARG	7	B	3.71
23	858	CD	GLN	110	A	<-->	2424	NH2	ARG	7	B	3.83
24	859	OE1	GLN	110	A	<-->	2418	CB	ARG	7	B	3.44
25	859	OE1	GLN	110	A	<-->	2419	CG	ARG	7	B	3.68
26	859	OE1	GLN	110	A	<-->	2420	CD	ARG	7	B	3.8
27	859	OE1	GLN	110	A	<-->	2421	NE	ARG	7	B	2.69
28	859	OE1	GLN	110	A	<-->	2422	CZ	ARG	7	B	3.4
29	859	OE1	GLN	110	A	<-->	2424	NH2	ARG	7	B	3.26
30	860	NE2	GLN	110	A	<-->	2416	N	ARG	7	B	3.69
31	863	N	THR	111	A	<-->	2424	NH2	ARG	7	B	3.09
32	864	CA	THR	111	A	<-->	2424	NH2	ARG	7	B	3.89
33	868	C	THR	111	A	<-->	2424	NH2	ARG	7	B	3.7
34	869	O	THR	111	A	<-->	2422	CZ	ARG	7	B	3.89
35	869	O	THR	111	A	<-->	2424	NH2	ARG	7	B	2.81
36	1019	CA	PRO	132	A	<-->	2364	CG	GLN	2	B	3.8
37	1021	CB	PRO	132	A	<-->	2364	CG	GLN	2	B	3.63
38	1021	CB	PRO	132	A	<-->	2365	CD	GLN	2	B	3.25
39	1021	CB	PRO	132	A	<-->	2366	OE1	GLN	2	B	3.23

40	1021	CB	PRO	132	A	<-->	2367	NE2	GLN	2	B	3.73
41	1155	CB	ASN	151	A	<-->	2492	OD2	ASP	14	B	3.9
42	1157	OD1	ASN	151	A	<-->	2422	CZ	ARG	7	B	3.68
43	1157	OD1	ASN	151	A	<-->	2423	NH1	ARG	7	B	3.25
44	1157	OD1	ASN	151	A	<-->	2424	NH2	ARG	7	B	3.74
45	1172	CG	ASP	153	A	<-->	2478	O	ARG	12	B	3.38
46	1172	CG	ASP	153	A	<-->	2475	NH1	ARG	12	B	3.81
47	1173	OD1	ASP	153	A	<-->	2478	O	ARG	12	B	2.94
48	1173	OD1	ASP	153	A	<-->	2470	CB	ARG	12	B	3.82
49	1173	OD1	ASP	153	A	<-->	2475	NH1	ARG	12	B	2.81
50	1174	OD2	ASP	153	A	<-->	2478	O	ARG	12	B	3.21
51	1212	CB	SER	158	A	<-->	2492	OD2	ASP	14	B	3.13
52	1213	OG	SER	158	A	<-->	2486	O	ASP	13	B	3.81
53	1213	OG	SER	158	A	<-->	2492	OD2	ASP	14	B	3.36
54	1505	CG2	THR	196	A	<-->	2358	NH2	ARG	1	B	3.16
55	1519	OG1	THR	198	A	<-->	2366	OE1	GLN	2	B	3.64
56	1541	OG1	THR	201	A	<-->	2379	OH	TYR	3	B	3.81
57	1548	CG1	VAL	202	A	<-->	2379	OH	TYR	3	B	3.27
58	1868	CB	GLU	240	A	<-->	2374	CD1	TYR	3	B	3.64
59	1868	CB	GLU	240	A	<-->	2376	CE1	TYR	3	B	2.98
60	1868	CB	GLU	240	A	<-->	2378	CZ	TYR	3	B	3.86
61	1869	CG	GLU	240	A	<-->	2376	CE1	TYR	3	B	3.25
62	1869	CG	GLU	240	A	<-->	2378	CZ	TYR	3	B	3.58
63	1869	CG	GLU	240	A	<-->	2379	OH	TYR	3	B	3.44
64	1870	CD	GLU	240	A	<-->	2374	CD1	TYR	3	B	3.61
65	1870	CD	GLU	240	A	<-->	2376	CE1	TYR	3	B	2.93
66	1870	CD	GLU	240	A	<-->	2377	CE2	TYR	3	B	3.77
67	1870	CD	GLU	240	A	<-->	2378	CZ	TYR	3	B	3.03
68	1870	CD	GLU	240	A	<-->	2379	OH	TYR	3	B	3.26
69	1871	OE1	GLU	240	A	<-->	2373	CG	TYR	3	B	3.48
70	1871	OE1	GLU	240	A	<-->	2374	CD1	TYR	3	B	2.93
71	1871	OE1	GLU	240	A	<-->	2375	CD2	TYR	3	B	3.84
72	1871	OE1	GLU	240	A	<-->	2376	CE1	TYR	3	B	2.76
73	1871	OE1	GLU	240	A	<-->	2377	CE2	TYR	3	B	3.73
74	1871	OE1	GLU	240	A	<-->	2378	CZ	TYR	3	B	3.21
75	1872	OE2	GLU	240	A	<-->	2376	CE1	TYR	3	B	3.6
76	1872	OE2	GLU	240	A	<-->	2377	CE2	TYR	3	B	3.66
77	1872	OE2	GLU	240	A	<-->	2378	CZ	TYR	3	B	3.19
78	1872	OE2	GLU	240	A	<-->	2379	OH	TYR	3	B	3.15
79	1880	C	PRO	241	A	<-->	2379	OH	TYR	3	B	3.7
80	1881	O	PRO	241	A	<-->	2376	CE1	TYR	3	B	3.52
81	1881	O	PRO	241	A	<-->	2378	CZ	TYR	3	B	3.4
82	1881	O	PRO	241	A	<-->	2379	OH	TYR	3	B	2.56
83	1877	CD	PRO	241	A	<-->	2350	N	ARG	1	B	3.79
84	1907	CA	ASP	245	A	<-->	2411	CE2	TYR	6	B	3.45

85	1907	CA	ASP	245	A	<-->	2412	CZ	TYR	6	B	3.79
86	1907	CA	ASP	245	A	<-->	2413	OH	TYR	6	B	3.31
87	1912	C	ASP	245	A	<-->	2409	CD2	TYR	6	B	3.8
88	1912	C	ASP	245	A	<-->	2411	CE2	TYR	6	B	2.94
89	1912	C	ASP	245	A	<-->	2412	CZ	TYR	6	B	3.4
90	1912	C	ASP	245	A	<-->	2413	OH	TYR	6	B	3.4
91	1913	O	ASP	245	A	<-->	2409	CD2	TYR	6	B	3.65
92	1913	O	ASP	245	A	<-->	2410	CE1	TYR	6	B	3.73
93	1913	O	ASP	245	A	<-->	2411	CE2	TYR	6	B	2.82
94	1913	O	ASP	245	A	<-->	2412	CZ	TYR	6	B	2.87
95	1913	O	ASP	245	A	<-->	2413	OH	TYR	6	B	2.92
96	1908	CB	ASP	245	A	<-->	2411	CE2	TYR	6	B	2.95
97	1908	CB	ASP	245	A	<-->	2412	CZ	TYR	6	B	3.53
98	1908	CB	ASP	245	A	<-->	2413	OH	TYR	6	B	3.23
99	1909	CG	ASP	245	A	<-->	2413	OH	TYR	6	B	3.86
100	1914	N	HIS	246	A	<-->	2411	CE2	TYR	6	B	3.5
101	1915	CA	HIS	246	A	<-->	2411	CE2	TYR	6	B	3.89
102	1940	CA	ILE	249	A	<-->	2432	CD2	TYR	8	B	3.89
103	1946	O	ILE	249	A	<-->	2429	CB	TYR	8	B	3.53
104	1946	O	ILE	249	A	<-->	2430	CG	TYR	8	B	3.78
105	1946	O	ILE	249	A	<-->	2432	CD2	TYR	8	B	3.81
106	1941	CB	ILE	249	A	<-->	2407	CG	TYR	6	B	3.64
107	1941	CB	ILE	249	A	<-->	2408	CD1	TYR	6	B	3.12
108	1941	CB	ILE	249	A	<-->	2410	CE1	TYR	6	B	3.32
109	1941	CB	ILE	249	A	<-->	2429	CB	TYR	8	B	3.66
110	1942	CG1	ILE	249	A	<-->	2408	CD1	TYR	6	B	3.59
111	1942	CG1	ILE	249	A	<-->	2427	N	TYR	8	B	3.55
112	1942	CG1	ILE	249	A	<-->	2428	CA	TYR	8	B	3.77
113	1942	CG1	ILE	249	A	<-->	2429	CB	TYR	8	B	2.93
114	1943	CG2	ILE	249	A	<-->	2406	CB	TYR	6	B	3.88
115	1943	CG2	ILE	249	A	<-->	2407	CG	TYR	6	B	3.17
116	1943	CG2	ILE	249	A	<-->	2408	CD1	TYR	6	B	3.2
117	1943	CG2	ILE	249	A	<-->	2409	CD2	TYR	6	B	3.35
118	1943	CG2	ILE	249	A	<-->	2410	CE1	TYR	6	B	3.4
119	1943	CG2	ILE	249	A	<-->	2411	CE2	TYR	6	B	3.54
120	1943	CG2	ILE	249	A	<-->	2412	CZ	TYR	6	B	3.56
121	1944	CD1	ILE	249	A	<-->	2406	CB	TYR	6	B	2.95
122	1944	CD1	ILE	249	A	<-->	2407	CG	TYR	6	B	3.22
123	1944	CD1	ILE	249	A	<-->	2408	CD1	TYR	6	B	3.02
124	1944	CD1	ILE	249	A	<-->	2416	N	ARG	7	B	3.52
125	1944	CD1	ILE	249	A	<-->	2425	C	ARG	7	B	3.88
126	1944	CD1	ILE	249	A	<-->	2427	N	TYR	8	B	2.84
127	1944	CD1	ILE	249	A	<-->	2428	CA	TYR	8	B	3.63
128	1944	CD1	ILE	249	A	<-->	2429	CB	TYR	8	B	3.4
129	1958	O	GLY	251	A	<-->	2432	CD2	TYR	8	B	3.86

130	1963	CG	PRO	252	A	<-->	2433	CE1	TYR	8	B	3.8
131	1961	CD	PRO	252	A	<-->	2433	CE1	TYR	8	B	3.59
132	1961	CD	PRO	252	A	<-->	2434	CE2	TYR	8	B	3.62
133	1961	CD	PRO	252	A	<-->	2435	CZ	TYR	8	B	3.42
134	1961	CD	PRO	252	A	<-->	2436	OH	TYR	8	B	3.84
135	2255	CG2	THR	292	A	<-->	2418	CB	ARG	7	B	3.43
136	2267	CB	PHE	294	A	<-->	2418	CB	ARG	7	B	3.73
137	2267	CB	PHE	294	A	<-->	2419	CG	ARG	7	B	3.32
138	2267	CB	PHE	294	A	<-->	2420	CD	ARG	7	B	2.94
139	2268	CG	PHE	294	A	<-->	2420	CD	ARG	7	B	3.62
140	2268	CG	PHE	294	A	<-->	2472	CD	ARG	12	B	3.75
141	2268	CG	PHE	294	A	<-->	2473	NE	ARG	12	B	3.35
142	2269	CD1	PHE	294	A	<-->	2473	NE	ARG	12	B	3.4
143	2270	CD2	PHE	294	A	<-->	2472	CD	ARG	12	B	3.51
144	2270	CD2	PHE	294	A	<-->	2473	NE	ARG	12	B	3.16
145	2271	CE1	PHE	294	A	<-->	2473	NE	ARG	12	B	3.29
146	2271	CE1	PHE	294	A	<-->	2474	CZ	ARG	12	B	3.77
147	2271	CE1	PHE	294	A	<-->	2476	NH2	ARG	12	B	3.36
148	2272	CE2	PHE	294	A	<-->	2472	CD	ARG	12	B	3.8
149	2272	CE2	PHE	294	A	<-->	2473	NE	ARG	12	B	3.04
150	2272	CE2	PHE	294	A	<-->	2474	CZ	ARG	12	B	3.52
151	2272	CE2	PHE	294	A	<-->	2476	NH2	ARG	12	B	3.63
152	2273	CZ	PHE	294	A	<-->	2473	NE	ARG	12	B	3.1
153	2273	CZ	PHE	294	A	<-->	2474	CZ	ARG	12	B	3.33
154	2273	CZ	PHE	294	A	<-->	2476	NH2	ARG	12	B	2.96
155	2280	OD1	ASP	295	A	<-->	2423	NH1	ARG	7	B	3.47
156	2306	NH2	ARG	298	A	<-->	2472	CD	ARG	12	B	3.74
157	2306	NH2	ARG	298	A	<-->	2473	NE	ARG	12	B	3.82
158	2306	NH2	ARG	298	A	<-->	2474	CZ	ARG	12	B	3.7
159	2306	NH2	ARG	298	A	<-->	2475	NH1	ARG	12	B	3.48

Table 6.7.C. *List of atom-atom interactions (Salt bridge) across protein-peptide interface in Mpro (Chain A) and Peptide4 (Chain B) complex from PDBsum server*

Mpro (Chain A)						Salt bridge	Peptide4 (Chain B)					
Sl.no.	Atom no.	Atom name	Res name	Res no.	Chain		Atom no.	Atom name	Res name	Res no.	Chain	Distance
1	1173	OD1	ASP	153	A	<-->	2475	NH1	ARG	12	B	2.81
2	2280	OD1	ASP	295	A	<-->	2423	NH1	ARG	7	B	3.47

6.3.6. Absorption, Distribution, Metabolism, Excretion, and Toxicity (ADMET) analysis

We also performed the ADMET (Absorption, Distribution, Metabolism, Excretion, and Toxicity) properties which is essential for assessing its potential as a drug candidate. We used the ADMETLab 2.0 [46] for the ADME prediction for peptide2 and peptide4. And the results are tabulated in **Table 6.8.**

Table 6.8. *ADME analysis of peptide 2 and peptide 4 using ADMETLab2.0 tool*

1. Physicochemical Property

Property	Value (peptide 2)	Value (peptide 4)
Molecular Weight (Da)	2304.08	2277.060
Volume ($Å^3$)	2225.304	2196.484
Log S (mol/L)	-1.153	-1.216
Log P	-9.39	-7.972
log D	-2.567	-2.796
nHA (Number of hydrogen bond acceptors)	64	62
nHD (Number of hydrogen bond donors)	49	49

2. Medicinal Chemistry

Property	Value (peptide2)	Value (peptide4)	Comments
Fsp3	0.47 (Accepted value)	0.469(Accepted value)	The number of sp3 hybridized carbons / total carbon count, correlating with melting point and solubility. Fsp3 ≥0.42 is considered a suitable value.
MCE-18	132.0 (Accepted value)	130.000(Accepted value)	MCE-18 stands for medicinal chemistry evolution. MCE-18≥45 is considered a suitable value.
Pfizer Rule	Accepted	Accepted	logP > 3; TPSA < 75 Compounds with a high log P (>3) and low TPSA (<75) are likely to be toxic.

3. Absorption

Property	Value (peptide2)	Value (peptide4)	Comments
MDCK Permeability	7e-06	3.7e-06	low permeability: < 2 × 10−6 cm/s medium permeability: 2–20 × 10−6 cm/s high passive permeability: > 20 × 10−6 cm/s
Pgp-inhibitor	0.0	0.0	Category 1: Inhibitor; Category 0: Non-inhibitor

4. Distribution

Property	Value (peptide2)	Value (peptide4)	Comments
PPB	45.72%	43.772%	Plasma Protein Binding Optimal: < 90%. Drugs with high protein-bound may have a low therapeutic index.
VD	0.639	0.503	Volume Distribution Optimal: 0.04-20L/kg
BBB Penetration Blood-	0.01	0.01	Brain Barrier Penetration Category 1: BBB+; Category 0: BBB-; The output value is the probability of being BBB+
Fu	33.05%	31.377%	The fraction unbound in plasms; Low:<5% ; Middle: 5-20%; High: > 20%

Hence, according to the above preliminary in-silico analysis, out of all 13 peptides we screened out 2 peptides (peptide 2 and peptide 4) and were subjected to the MD simulation followed by various analysis.

6.3.7. MD Simulation

Energy minimization constituting of the steepest descent method, followed by conjugate gradient minimization was carried out for the Mpro Apoprotein and the two selected protein-peptide complexes (Mpro-peptide2 complex and Mpro-peptide4 complex). The energy minimisation was the followed by the MD simulation which was performed using the AMBER ff99SB force field and AMBER software programme [47-50] for the Mpro Apoprotein along with the two complex system. The force field is a collection of equations and associated constants designed to reproduce molecular geometry and selected properties of tested structures [51]. More specifically, the functional form and parameter sets utilised to determine the potential energy of an atomistic system are referred to as the force field [51]. The TIP3P water model is designed to be used with the ff99SB force field. The backbone parameters included a TIP3P-specific correction and were based on alanine and glycine [51].

The basic functional form of potential energy used in modelling molecular systems includes intramolecular interaction terms that describe the interactions of atoms connected by covalent bonds, and the intermolecular (i.e., nonbonded, also termed noncovalent) terms describe the long-range electrostatic and van der Waals forces. The specific decomposition of the terms depends on the force field, but a general form for the total energy in an additive force field can be written as:

$$E_{total} = E_{bonded} + E_{nonbonded}$$

where the components of the covalent and noncovalent contributions are given by the following summations:

$$E_{bonded} = E_{bond} + E_{angle} + E_{dihedral}$$

$$E_{nonbonded} = E_{electrostatic} + E_{van\ der\ waals}$$

The force field energy terms can also be described as:

$$E_{FF} = E_{STRETCH} + E_{BEND} + E_{TORS} + E_{VDW} + E_{ELE} + E_{CROSS}$$

An appropriate number of counter ions have been added in order to ensure the overall neutrality of both the two complex systems and Mpro Apoprotein. All the systems were solvated with the TIP3P water model with an explicit solvent and a solvent buffer of 10 Å in all directions [52]. Water clusters, liquid water, and aqueous solutions with an explicit solvent are all simulated and thermodynamically calculated in computational studies employing a water model. Quantum mechanics, molecular mechanics, experimental data, and a combination of these are used to determine the models. Numerous models have been constructed that imitate specific molecular properties; in the present study, we have employed the TIP3P water model. The TIP3P water model is conventionally used in molecular dynamics because of the optimization of its parameters to protein-protein interactions [51]. Then, Mpro and the two peptides (peptides 2 and 4) were set at 500 kcal/mol/Å^2. and the energy of all water molecules and counterions present in the entire system was minimised for 10,000 steps of steepest descents (SD) and then for 10,000 steps of conjugate gradient (CG). Now in order to eliminate the conflicting contacts from the Mpro Apoprotein along with the two complex system, the CG minimization was carried out and this process was continued for 8000 steps for CG minimization and 12000 steps for SD minimization. Subsequently, three rounds of 3000 ps equilibration with a force constant of 5.0 kcal/mol/Å^2 are applied to both the complex systems and the Mpro Apoprotein. After that, the solute atoms are subjected to harmonic constraints with a force constant of 10 kcal/mol/Å^2, and the process was gradually heated under constant volume (NVT) conditions from 0 to 300 K. After that, 200 ns of MD simulations were performed without constraint using the NPT ensemble.

To address the long-range electrostatic interactions, we constrained the direct space sum using the Particle Mesh Ewald [54] approach, with a non-bonded cutoff of 12.0. All the bonds that were present in the entire system were constrained using the SHAKE algorithm [54]. In MD simulations the need often arises to

maintain such parameters as temperature or pressure rather than energy and volume, or to impose gradients for studying transport properties in MD [55]. Weak coupling to an external bath, uses the principle of least local perturbation consistent with the required global coupling. This approximates the perturbation that would occur in an ideal physical nonequilibrium experiment. A simulated system is loosely coupled to a constant temperature and/or pressure bath using the Berendsen weak coupling approach, which has been proven to be reliable and easy to implement. It offers an accurate algorithm that eliminates the need for intermediate adjustments and enables seamless transitions to new pressure or temperature values. Throughout the simulation, the temperature and pressure were maintained at constants (0.5 ps for the heat bath and 0.2 ps for pressure relaxation) by the Berendsen weak coupling approach [55]. Using a time step of 2 fs MD simulation, the MD file was sampled every 10 ps.

6.3.8. Analysis of MD simulation trajectories

The conformational dynamics and other significant structural characteristics of the Mpro Apoprotein and its two complexes (Mpro-peptide2 and Mpro-peptide4) have been analysed using the corresponding 200 ns MD trajectory files. Our study includes the following analysis: RMSD, RMSF, inter molecular hydrogen bond analysis and were carried out using cpptraj module [56] of AMBER software package and xmgrace plotting tool was used for generating the plots.

Snapshots of Mpro Apoprotein along with the Mpro-peptide2 and Mpro-peptide4 complex structures at discrete time interval during the 200 ns of MD simulation as shown in **Figure 6.6, 6.7 and 6.8** respectively.

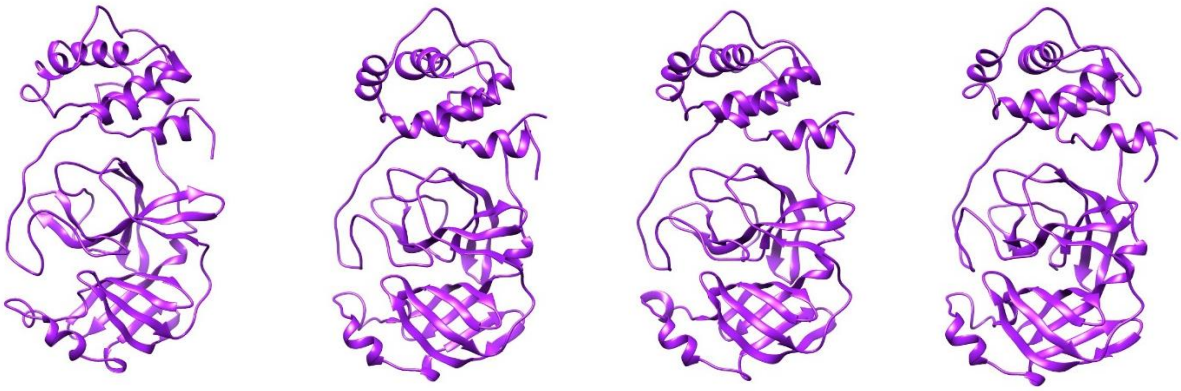

0 ns **10 ns** **20 ns** **40 ns**

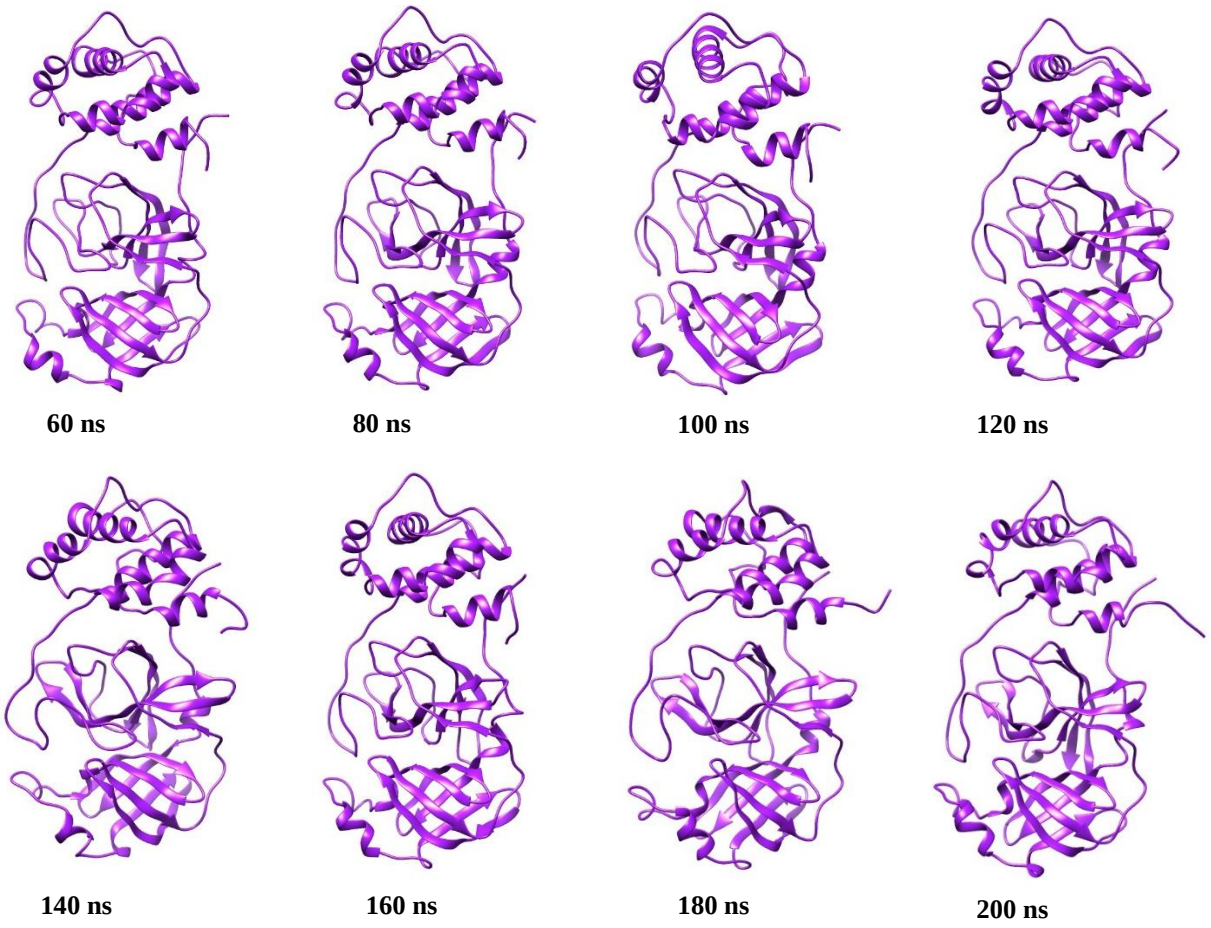

Figure 6.6. *Snapshots of SARS-CoV-2 Mpro apoprotein structures at discrete time interval during the 200 ns MD simulation*

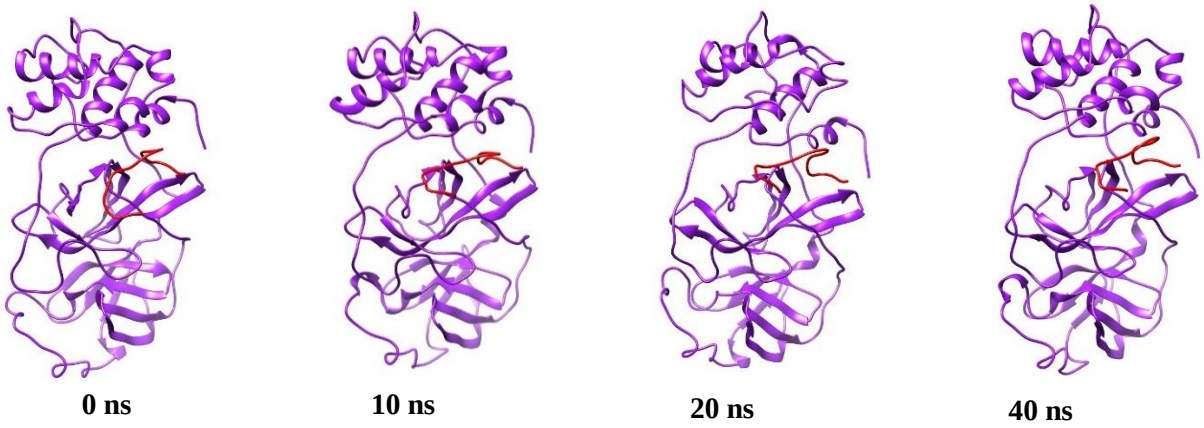

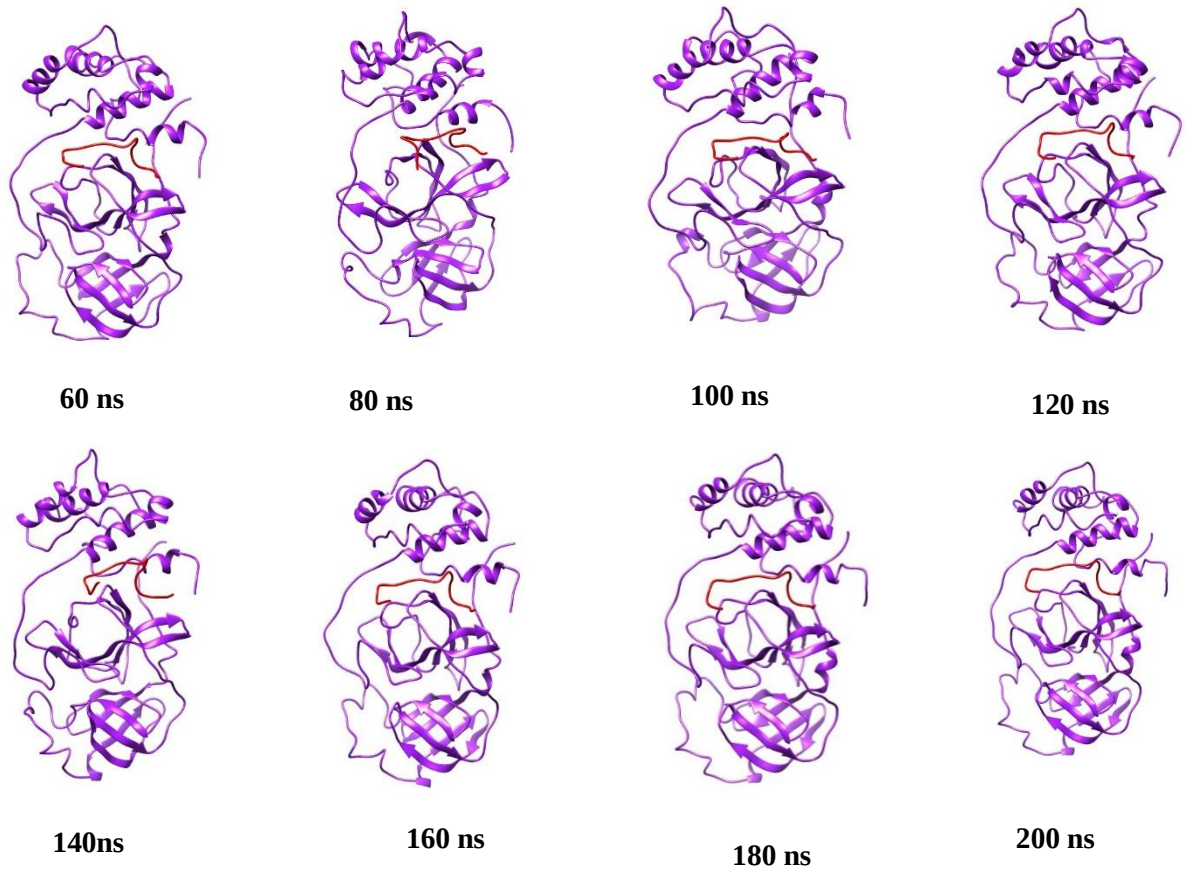

Figure 6.7. *Snapshots of SARS-CoV-2 Mpro-peptide2 complex structures at discrete time interval during the 200 ns MD simulation.*

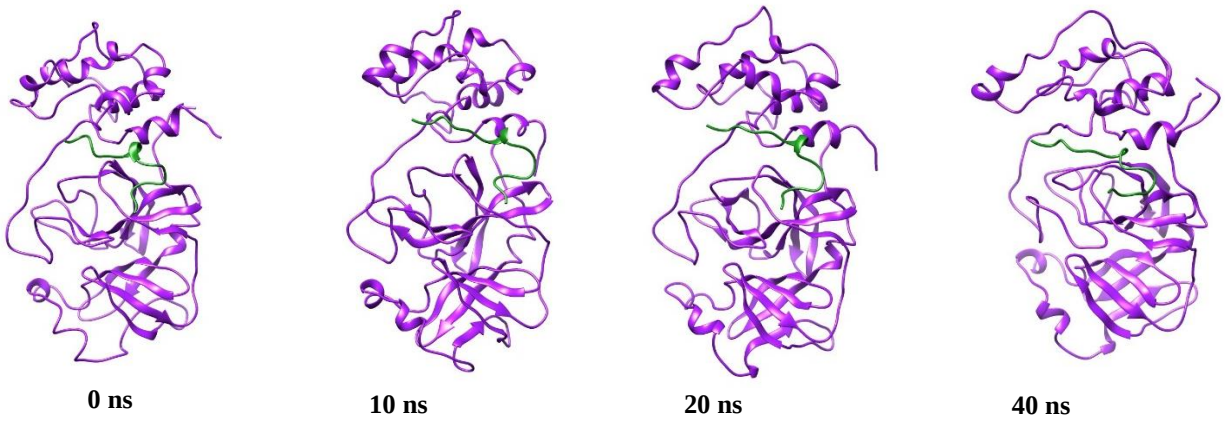

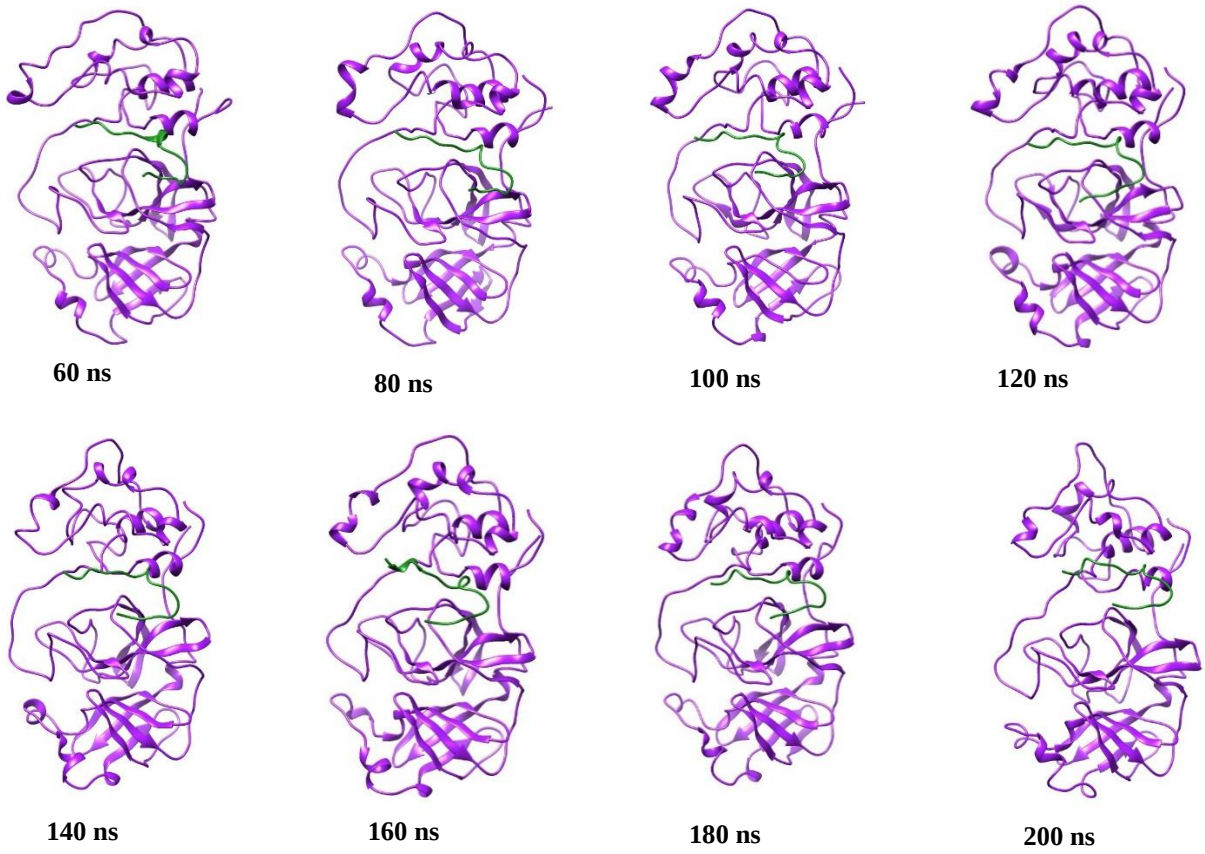

Figure 6.8. *Snapshots of SARS-CoV-2 Mpro-peptide4 complex structures at discrete time interval during the 200 ns MD simulation.*

6.3.9. Binding Free energy calculations

Molecular Mechanics Generalised Born Surface Area (MM-GBSA) technique implemented in AMBER 16 [57, 58] package was used to determine the binding free energy and free energy decomposition of the two complex systems (Mpro-peptide2 and Mpro-peptide4). For each complex system, 200 snapshots were selected from the last 10 ns of MD trajectories to calculate the relevant energies.

The rest of the steps were performed as mention in section **5.3.5** and **5.3.6 of Chapter 5** [59-71].

In order to get more insight in to the residue level, energy decompositions were performed within the two complex systems. Here, only per-residue decomposition was included. In this case, the energy contribution of each residue from the combination of Protein (Mpro) with the ligand (peptide) was divided into three terms: van der Waals contribution (ΔE_{vdW}), electrostatic contribution (ΔEele), and solvation contribution ($\Delta G_{GB} + \Delta G_{SA}$).

The summary of the methodology is depicted in **Figure 6.9.**

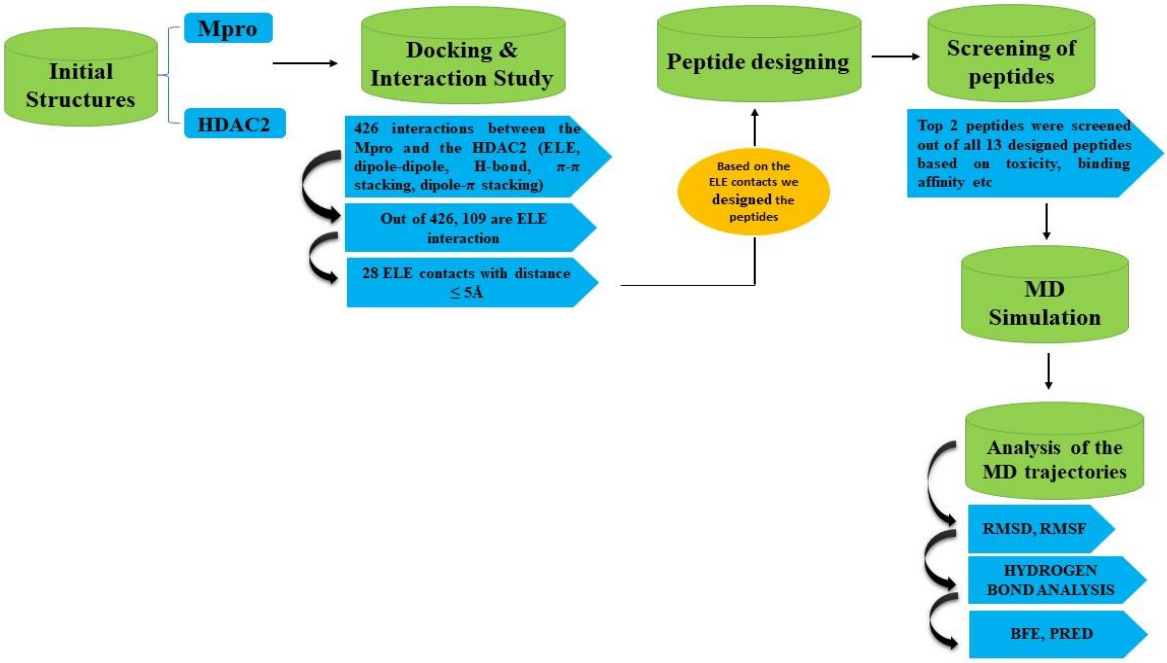

Figure 6.9. *The summary of the methodology used in this work in the form of a flowchart.*

6.4. Result and discussion:

6.4.1. Root mean square deviation (RMSD)

Now in order the test the stability of the two complex systems (Mpro-peptide2 and Mpro-peptide4), we analysed the trajectories generated from the 200 ns MD simulation. First, we performed the RMSD analysis. Root mean square deviation (RMSD) is used to measure the difference between the backbones of a protein from its initial structural conformation to its final conformation. The stability of the protein relative to its conformation can be determined by the deviations produced during the course of its simulation. The smaller the deviations, the more stable the protein structure.

The RMSD (root mean square deviation) values of the backbone atoms of the complexes were calculated to depict the average deviations in the atomic positions and the stability of the complexes and apoprotein through the trajectories of 200 ns of the MD simulations **(Figure 6.10).** The RMSD of both the complexes appeared to be stable after 10 ns simulation which reveals that each of the system has achieved good convergence. Interestingly, we also noticed that the RMSD values of both the complexes depicts a lower value and observed to be stable when compared to the Mpro Apoprotein. The average of RMSD was calculated to be **1.55 Å (± 0.12)** for the Mpro-peptide2 complex structure and **2.58 Å (± 0.14)** for the Mpro-peptide4 complex structure, which indicates that the Mpro-peptide2 complex structure has a greater stability as compared to the Mpro-peptide4 complex.

Moreover, we also test the stability of the Mpro Apoprotein that is the unbound state of the target protein and interestingly we found that the stability of the Mpro increases significantly when bound to the peptides. The average RMSD of the Mpro Apoprotein was found to be **3.31 Å (± 0.12)**, which is comparatively less stable than the bound state (complex form).

The RMSD of the Mpro Apoprotein and the Mpro-peptide2 and Mpro-peptide4 complex systems are shown in **Figure 6.10.**

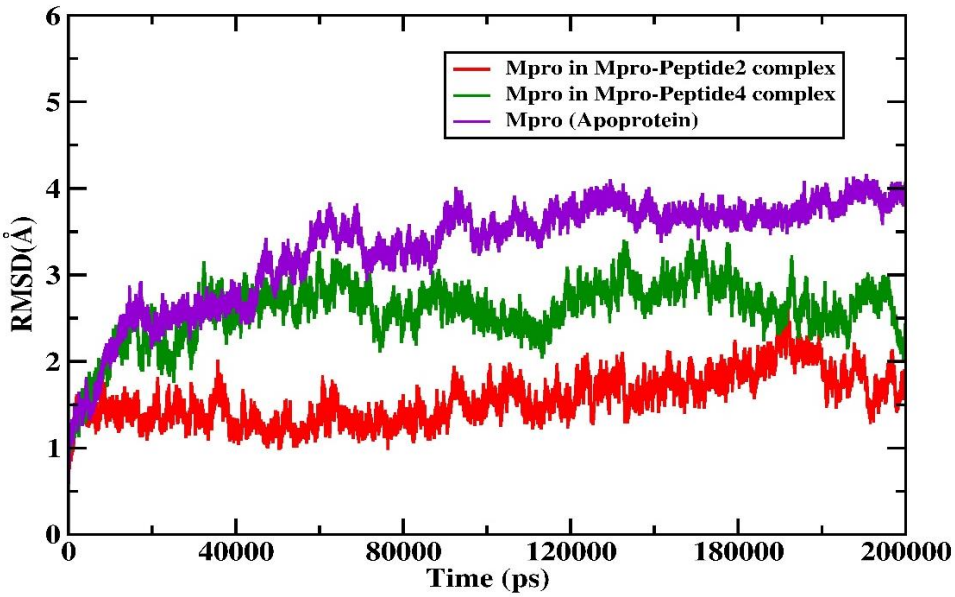

Figure 6.10. *Backbone RMSD's for Mpro Apoprotein (violet), Mpro in Mpro-peptide4 complex (green) and Mpro in Mpro-peptide2 complex (red)*

6.4.2. Root mean square fluctuation (RMSF)

RMSF is a numerical measurement similar to RMSD, but instead of indicating positional differences between entire structures over time, RMSF is a calculation of individual residue flexibility, or how much a particular residue fluctuates during the simulation period. RMSF per residue is typically plotted vs. residue number and can indicate structurally which amino acids in a protein contribute the most to its extend of flexibility or rigidness.

By computing the Cα RMSF values from the MD simulations trajectory analysis, we analyzed the flexibility of Mpro in both complexes (Mpro-peptide2 and Mpro-peptide4) and also compared it with the flexibility of the Mpro Apoprotein. The average RMSF was found to be **0.78 Å** for the Mpro-peptide2 complex and that too for the Mpro-peptide4 complex was found to be **2.95 Å**. The average RMSF for the Mpro Apoprotein was found to be **4.59 Å** which shows that the Mpro attains a significantly higher stability when bound to the peptides. In **Figure 6.11,** the RMSF analysis of the Mpro Apoprotein along with the Mpro in both the complex system are depicted. We observed that the structure of Mpro in (Mpro-peptide2)

and (Mpro-peptide4) complexes becomes relatively stable with lesser fluctuation when compared with the Mpro Apoprotein. Hence inferring a greater stability to the Mpro when bound to the peptides than in the unbound form (Mpro Apoprotein). We also analyzed the fluctuation in the active site resides that are interacting with the peptide. We found that the active site resides are more flexible in the Mpro Apoprotein and its significantly losses its flexibility and became more rigid when bound to the peptides thereby increasing the stability of the complexes compared to the Apoprotein.

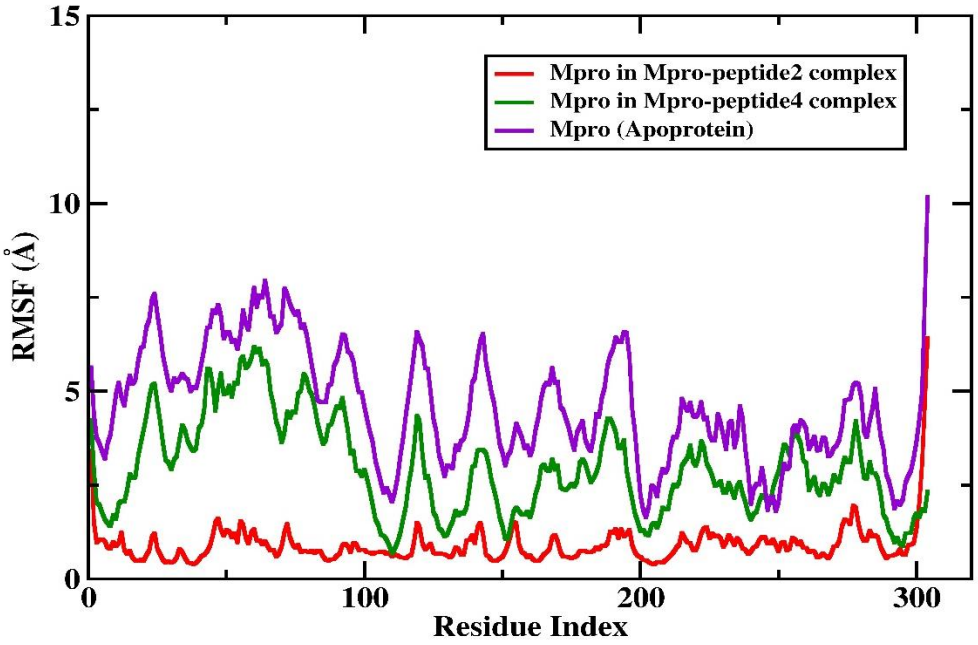

Figure 6.11. *Backbone RMSF's for Mpro in Apoprotein (purple), Mpro-peptide4 complex (green) and Mpro-peptide2 complex (red).*

6.4.3. Hydrogen bond analysis

The number of hydrogen bonds present in (Mpro-peptide2) and (Mpro-peptide4) complexes were calculated (**Figure 6.12**), as these hydrogen bonds is responsible for conferring stability to the protein complexes. The number of intermolecular hydrogen bonds was found to be higher in Mpro-peptide2 complex than the Mpro-peptide4 complex. The entire list of intermolecular hydrogen bonds formed between the Mpro-peptide2 (acceptor/donor) and Mpro-peptide4 complex (donor/acceptor) during the last 20 ns of the 200 ns MD simulation for both the complexes were summarized in **Table 6.9-6.12.**

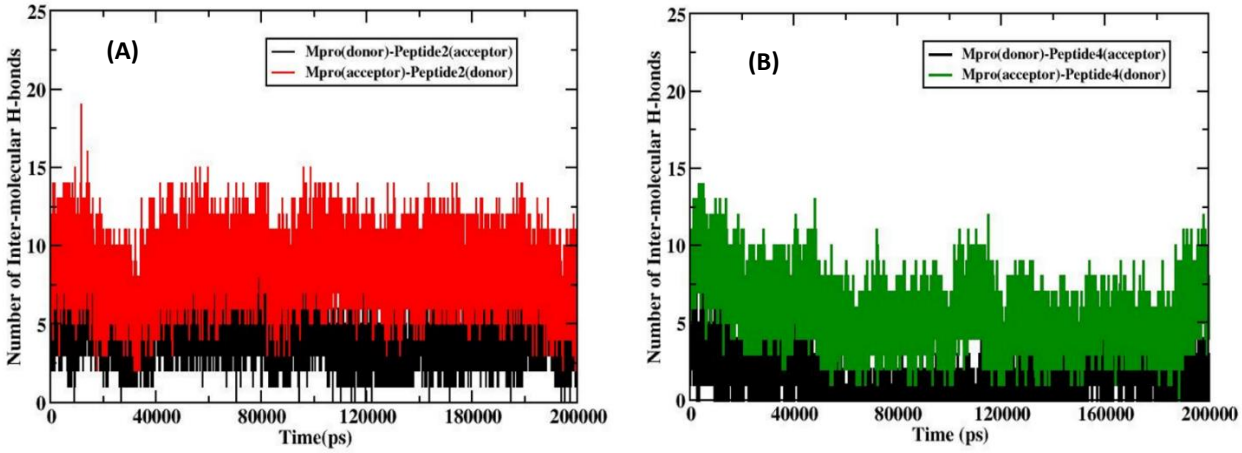

Figure 6.12. *The number of intermolecular hydrogen bonds between* ***(A)*** *Mpro-peptide2 complex (Red-black) and* ***(B)*** *Mpro-peptide4 complex (Green-black)*

Table 6.9: *Hydrogen bond analysis of Mpro-Peptide2 complex during the last 20 ns of MD simulation with Mpro as acceptor and peptide2 as donor.*

#Acceptor	DonorH	Donor	Frac	Average Distance (Å)	Average Angles (°)
GLN_308@OE1	SER_113@HG	SER_113@OG	0.9296	2.7345	162.7261
GLN_308@O	THR_292@HG1	THR_292@OG1	0.6175	2.7671	161.1176
ASP_320@O	ARG_105@HH22	ARG_105@NH2	0.223	2.8062	158.4748
ASP_319@OD1	GLN_107@HE21	GLN_107@NE2	0.1652	2.8344	156.869
GLN_308@HB2	ASN_151@HD21	ASN_151@ND2	0.1645	2.753	145.8016
ASP_320@OXT	GLN_107@HE21	GLN_107@NE2	0.1595	2.8233	161.0861
TYR_310@HB2	GLN_110@HE21	GLN_110@NE2	0.1103	2.8253	146.9542
ASP_319@OD2	ARG_105@HH22	ARG_105@NH2	0.1102	2.8271	157.5208
GLN_308@O	THR_111@HG1	THR_111@OG1	0.1083	2.7044	154.4267
ASP_320@OXT	ARG_105@HH12	ARG_105@NH1	0.1066	2.8227	157.0955
ASP_319@OD2	ARG_105@HH12	ARG_105@NH1	0.0986	2.8133	157.0517
ASP_320@O	ARG_105@HH12	ARG_105@NH1	0.097	2.8241	155.8968
ASP_320@OXT	ARG_105@HH22	ARG_105@NH2	0.0962	2.8147	156.3748
ASP_319@OD1	ARG_105@HH22	ARG_105@NH2	0.0703	2.8328	158.556
ASP_319@OD2	GLN_107@HE21	GLN_107@NE2	0.0701	2.8432	156.1042
ASP_320@OD2	ARG_105@HH12	ARG_105@NH1	0.0612	2.8129	155.5685
ASP_319@OD1	ARG_105@HH12	ARG_105@NH1	0.0487	2.8221	157.8537
ASP_320@OD1	ARG_105@HH12	ARG_105@NH1	0.0407	2.8133	155.4532
GLU_306@OE1	SER_158@HG	SER_158@OG	0.0379	2.6528	166.244
ASP_320@O	GLN_107@HE21	GLN_107@NE2	0.0375	2.8368	156.2968
ARG_307@HH12	TYR_154@HA	TYR_154@CA	0.0366	2.8975	143.5541
GLN_308@OE1	GLN_127@HE22	GLN_127@NE2	0.0293	2.856	159.9992
GLU_306@HB3	ASN_151@HD21	ASN_151@ND2	0.0264	2.736	149.1385
ASP_320@OD2	GLN_107@HE21	GLN_107@NE2	0.0251	2.8189	161.9225

ARG_313@HB3	GLN_107@HE21	GLN_107@NE2	0.0241	2.7422	146.9982
TYR_309@OH	GLN_107@H	GLN_107@N	0.0218	2.9155	149.1635
TYR_314@O	GLN_110@HE21	GLN_110@NE2	0.0213	2.8599	152.6758
GLN_308@O	ASN_151@HD21	ASN_151@ND2	0.0204	2.8754	158.1717
ASP_319@OD1	GLN_107@HE22	GLN_107@NE2	0.0187	2.8485	160.1965
ASP_320@OD2	GLN_107@HE22	GLN_107@NE2	0.0186	2.8269	156.9767
ASP_319@OD1	ARG_105@HH21	ARG_105@NH2	0.0169	2.7843	154.3686
ARG_307@HD2	ARG_298@HG2	ARG_298@CG	0.0157	2.9372	144.7019
GLN_308@HG2	ARG_298@HD2	ARG_298@CD	0.0154	2.9355	141.0404
ASP_320@OD1	GLN_107@HE22	GLN_107@NE2	0.0148	2.8211	157.4648
ASP_319@OD2	GLN_107@HE22	GLN_107@NE2	0.0147	2.8494	160.4824
ASP_320@OD2	ARG_105@HH22	ARG_105@NH2	0.014	2.8147	154.8982
TYR_310@HH	VAL_202@HB	VAL_202@CB	0.0132	2.9166	143.8074
ASP_320@OD1	ARG_105@HH22	ARG_105@NH2	0.0126	2.8152	152.5964
TYR_309@HB3	GLN_110@HE21	GLN_110@NE2	0.0126	2.8249	143.1688
ASP_319@O	ARG_105@HE	ARG_105@NE	0.0124	2.8489	154.5485
TYR_309@CE2	ASN_151@HD22	ASN_151@ND2	0.0099	2.947	142.7182
ARG_316@HD3	PRO_108@HB2	PRO_108@CB	0.0096	2.9467	146.0278
TYR_309@O	PHE_294@H	PHE_294@N	0.0096	2.8862	152.9803
GLN_308@HE21	GLN_127@HG3	GLN_127@CG	0.0094	2.8744	140.0932
ARG_316@HH12	ILE_200@HB	ILE_200@CB	0.0077	2.93	144.4095
TYR_312@OH	HIE_246@HE2	HIE_246@NE2	0.0072	2.8946	147.9626
TYR_309@HE2	ASN_151@HD22	ASN_151@ND2	0.0068	2.9067	143.4916
ARG_307@HA	PHE_294@HE1	PHE_294@CE1	0.0067	2.9397	141.7511
TYR_312@H	ILE_249@HD11	ILE_249@CD1	0.0067	2.8308	150.4708
TYR_309@HB2	ASN_151@HD21	ASN_151@ND2	0.0062	2.8073	147.0969
ASP_320@OD1	GLN_107@HE21	GLN_107@NE2	0.006	2.8303	159.7524
HIE_311@HE1	PRO_293@HB2	PRO_293@CB	0.0059	2.9369	143.476
GLU_306@OE1	LYS_102@HZ1	LYS_102@NZ	0.0057	2.8022	159.6873
GLN_308@HE22	ARG_298@HH11	ARG_298@NH1	0.0056	2.8965	139.0479
ASP_320@OXT	ARG_105@HH21	ARG_105@NH2	0.0054	2.8194	152.7003
ARG_307@HG3	ARG_298@HD2	ARG_298@CD	0.0054	2.9419	141.5694
GLN_308@HB3	THR_111@HB	THR_111@CB	0.0051	2.9421	140.4666

Table 6.10: *Hydrogen bond analysis of Mpro-Peptide2 complex during the last 20 ns of MD simulation with peptide2 as acceptor and Mpro as donor.*

#Acceptor	**DonorH**	**Donor**	**Frac**	**Average Distance (Å)**	**Average Angles (º)**
ILE_152@O	ARG_307@H	ARG_307@N	0.8207	2.848	163.1459
ASP_295@OD2	GLN_308@HE22	GLN_308@NE2	0.5741	2.8163	162.9907
GLN_110@OE1	TYR_310@H	TYR_310@N	0.5593	2.8678	161.8732
GLU_240@OE1	ARG_316@HH12	ARG_316@NH1	0.5307	2.7835	159.2683
THR_304@O	ARG_307@HH12	ARG_307@NH1	0.523	2.7922	154.9023
GLU_240@OE2	ARG_316@HH22	ARG_316@NH2	0.5082	2.8099	160.8595

ARG_105@O	TYR_309@HH	TYR_309@OH	0.4663	2.7606	155.7088
GLU_240@OE2	ARG_316@HH12	ARG_316@NH1	0.3705	2.7829	158.2964
GLU_240@OE1	ARG_316@HH22	ARG_316@NH2	0.3696	2.809	160.1677
THR_304@O	ARG_307@HH22	ARG_307@NH2	0.2977	2.8238	150.1016
THR_304@OXT	ARG_307@HH22	ARG_307@NH2	0.257	2.8051	156.1186
THR_304@OXT	ARG_307@HH21	ARG_307@NH2	0.2246	2.7797	157.3385
ASP_295@OD1	GLN_308@HE22	GLN_308@NE2	0.217	2.8158	162.7634
ASN_151@HD21	GLN_308@HB2	GLN_308@CB	0.1948	2.8441	154.3558
ASP_153@OD2	GLU_305@H2	GLU_305@N	0.1779	2.7932	157.31
ASP_153@OD2	GLU_305@H3	GLU_305@N	0.1446	2.7965	156.9518
ASN_151@OD1	GLN_308@H	GLN_308@N	0.1392	2.9067	155.4567
ASP_153@OD1	GLU_305@H2	GLU_305@N	0.1232	2.7938	156.4694
GLN_107@OE1	ARG_313@HH11	ARG_313@NH1	0.1221	2.8378	153.5602
ASP_153@OD1	GLU_305@H1	GLU_305@N	0.118	2.7905	155.8379
ASP_153@OD2	GLU_305@H1	GLU_305@N	0.1132	2.8021	156.8893
THR_304@O	ARG_307@HE	ARG_307@NE	0.1091	2.8418	155.603
ASP_153@OD1	GLU_305@H3	GLU_305@N	0.1034	2.8033	155.6754
GLN_107@OE1	ARG_313@HH12	ARG_313@NH1	0.0934	2.8351	154.4059
GLN_110@HE21	TYR_310@HB2	TYR_310@CB	0.0782	2.8749	157.1491
GLN_127@OE1	GLN_308@HE21	GLN_308@NE2	0.0775	2.8502	144.1681
ASP_245@OD1	TYR_310@HH	TYR_310@OH	0.0773	2.7157	166.3606
THR_304@OXT	ARG_307@HH12	ARG_307@NH1	0.0741	2.8019	151.3087
ASP_245@OD2	TYR_310@HH	TYR_310@OH	0.069	2.7096	165.5743
GLN_127@HG3	GLN_308@HE21	GLN_308@NE2	0.0626	2.8812	147.824
GLN_110@OE1	TYR_314@H	TYR_314@N	0.0488	2.8742	157.6428
GLN_107@OE1	TYR_314@H	TYR_314@N	0.0479	2.8593	159.8915
VAL_104@O	TYR_309@HH	TYR_309@OH	0.0461	2.8123	158.353
THR_304@OXT	ARG_307@HE	ARG_307@NE	0.0446	2.8537	147.6741
VAL_202@O	TYR_310@HH	TYR_310@OH	0.042	2.8205	145.1035
ASN_151@HD21	GLU_306@HB3	GLU_306@CB	0.0369	2.8358	151.6178
GLY_251@O	TYR_312@HH	TYR_312@OH	0.036	2.7655	159.4069
TYR_154@HA	ARG_307@HH12	ARG_307@NH1	0.0281	2.8648	140.9776
GLN_107@OE1	TYR_309@HH	TYR_309@OH	0.0264	2.8033	158.2043
GLN_107@HE21	ARG_313@HB3	ARG_313@CB	0.023	2.8282	156.5264
ASN_151@OD1	GLN_308@HE22	GLN_308@NE2	0.0229	2.8483	159.3148
ARG_298@HH11	GLN_308@HE22	GLN_308@NE2	0.0218	2.8991	140.1284
GLU_240@OE2	ARG_316@HH11	ARG_316@NH1	0.0169	2.7979	153.7944
GLN_110@HE21	TYR_309@HB3	TYR_309@CB	0.0164	2.8843	146.4939
ARG_298@HG2	ARG_307@HD2	ARG_307@CD	0.0137	2.9322	141.5105
SER_113@OG	GLN_308@HE21	GLN_308@NE2	0.0136	2.8942	144.3954
THR_304@O	ARG_307@HH21	ARG_307@NH2	0.0132	2.8345	153.6948
ARG_298@HD2	GLN_308@HG2	GLN_308@CG	0.0123	2.944	144.3034
ILE_249@HD11	TYR_312@H	TYR_312@N	0.0118	2.8219	153.7988
GLN_107@OE1	ARG_316@H	ARG_316@N	0.0098	2.8875	163.3019
GLN_110@HG2	TYR_310@H	TYR_310@N	0.0098	2.8565	150.26

PHE_294@HE1	ARG_307@HA	ARG_307@CA	0.0098	2.9421	144.2169
ASN_151@HD21	TYR_309@HB2	TYR_309@CB	0.0088	2.893	153.8025
THR_304@C	ARG_307@HH22	ARG_307@NH2	0.0086	2.9585	147.9243
PRO_108@HB2	ARG_316@HD3	ARG_316@CD	0.0078	2.9297	141.6734
ASN_151@HD21	GLN_308@H	GLN_308@N	0.0074	2.8532	141.2069
ILE_249@HD12	TYR_312@H	TYR_312@N	0.0074	2.8314	155.6519
GLU_240@OE2	GLN_317@HE21	GLN_317@NE2	0.007	2.8519	157.4062
ASP_245@OD2	LYS_315@HZ1	LYS_315@NZ	0.0067	2.8221	154.5394
ASP_245@OD1	LYS_315@HZ3	LYS_315@NZ	0.0067	2.7912	154.4362
ILE_249@O	HIE_311@HE2	HIE_311@NE2	0.0063	2.8612	153.8495
ASP_245@OD2	LYS_315@HZ2	LYS_315@NZ	0.0062	2.8273	156.6488
GLN_107@NE2	TYR_309@HH	TYR_309@OH	0.0055	2.849	157.8574
GLU_240@OE1	GLN_317@HE21	GLN_317@NE2	0.0055	2.8489	158.5199
THR_111@HG1	GLN_308@HB3	GLN_308@CB	0.0052	2.8914	141.8271
ASP_155@OD2	ARG_307@HH21	ARG_307@NH2	0.0052	2.8255	155.6867
PRO_293@HB2	HIE_311@HE1	HIE_311@CE1	0.005	2.9341	143.3997

Table 6.11: *Hydrogen bond analysis of Mpro-Peptide4 complex during the last 20 ns of MD simulation with Mpro as acceptor and peptide4 as donor.*

#Acceptor	DonorH	Donor	Frac	Average Distance (Å)	Average Angles (°)
TYR_307@O	HIE_246@HE2	HIE_246@NE2	0.2914	2.8388	159.031
ASP_318@O	GLN_110@HE21	GLN_110@NE2	0.206	2.8589	158.5157
GLN_319@OE1	ARG_105@HH11	ARG_105@NH1	0.1982	2.8329	158.327
GLN_319@O	ARG_105@H	ARG_105@N	0.1131	2.8706	162.2106
ASP_318@OD2	ASN_151@HD22	ASN_151@ND2	0.0639	2.8146	156.6183
GLN_319@OE1	GLN_107@HE22	GLN_107@NE2	0.0627	2.8621	160.0225
ASP_317@OD1	LYS_102@HZ1	LYS_102@NZ	0.0371	2.7809	159.0263
ASP_317@OD1	LYS_102@HZ3	LYS_102@NZ	0.031	2.7872	158.8459
ASP_317@OD1	LYS_102@HZ2	LYS_102@NZ	0.024	2.7973	158.4592
ARG_316@O	LYS_102@HZ2	LYS_102@NZ	0.0213	2.8246	154.5306
ARG_316@O	LYS_102@HZ3	LYS_102@NZ	0.0199	2.827	154.9854
ARG_316@O	LYS_102@HZ1	LYS_102@NZ	0.0194	2.8274	155.439
ASP_318@OD1	GLN_110@HE21	GLN_110@NE2	0.0193	2.8501	156.9641
TYR_307@OH	THR_243@HG1	THR_243@OG1	0.0176	2.8404	155.2824
CYS_320@OXT	ARG_105@HH11	ARG_105@NH1	0.0157	2.8231	155.8691
TYR_307@HD1	THR_201@HB	THR_201@CB	0.0149	2.9385	143.7328
ARG_311@HD3	PHE_294@HD2	PHE_294@CD2	0.0132	2.9415	146.0919
ASP_318@H	VAL_104@HG12	VAL_104@CG1	0.0108	2.8691	142.2848
ASP_317@OD2	LYS_102@HZ1	LYS_102@NZ	0.0107	2.79	156.3895
ASP_317@OD2	LYS_102@HZ2	LYS_102@NZ	0.0106	2.7918	157.2042
HIE_309@O	GLN_107@HE22	GLN_107@NE2	0.0089	2.8684	150.9612
ARG_316@O	SER_158@HG	SER_158@OG	0.0087	2.7641	163.2987
GLN_319@HB3	ARG_105@HB2	ARG_105@CB	0.0086	2.945	143.2899

GLN_319@HA	GLN_110@HE21	GLN_110@NE2	0.0082	2.8228	144.1007
CYS_320@O	ARG_105@HH11	ARG_105@NH1	0.0076	2.8121	152.044
ARG_311@HD2	GLN_110@HG2	GLN_110@CG	0.0069	2.9416	143.5183
ARG_305@HG2	GLU_240@HG2	GLU_240@CG	0.0068	2.9458	143.3276
TYR_312@HB2	PHE_294@HB2	PHE_294@CB	0.006	2.9519	142.277
ASP_317@OD2	LYS_102@HZ3	LYS_102@NZ	0.0059	2.7912	155.5563
HIE_309@HE2	GLN_110@HE21	GLN_110@NE2	0.0058	2.892	144.5426
GLN_319@OE1	ARG_105@H	ARG_105@N	0.0057	2.8611	161.5867
ARG_305@HD2	GLU_240@HG2	GLU_240@CG	0.0051	2.9383	142.6403

Table 6.12: *Hydrogen bond analysis of Mpro-Peptide4 complex during the last 20 ns of MD simulation with peptide4 as acceptor and Mpro as donor.*

#Acceptor	DonorH	Donor	Frac	Average Distance (Å)	Average Angles (º)
PRO_241@O	TYR_307@HH	TYR_307@OH	0.8519	2.7273	163.3918
ASP_295@OD2	ARG_311@HH11	ARG_311@NH1	0.7537	2.7952	158.7336
GLU_240@OE1	GLN_306@H	GLN_306@N	0.5976	2.7846	157.9029
THR_111@O	ARG_311@HH12	ARG_311@NH1	0.4861	2.826	154.2301
GLU_240@OE2	GLN_306@H	GLN_306@N	0.281	2.7654	157.203
GLU_240@OE1	TYR_307@H	TYR_307@N	0.2044	2.8922	159.9201
ASN_231@OD1	ARG_305@HH22	ARG_305@NH2	0.1587	2.818	156.071
TYR_239@O	ARG_305@HH21	ARG_305@NH2	0.1565	2.8188	149.6801
ASP_245@OD1	TYR_308@HH	TYR_308@OH	0.1408	2.6921	162.4093
THR_111@O	ARG_311@HH22	ARG_311@NH2	0.1318	2.843	146.7675
TYR_239@O	ARG_305@HE	ARG_305@NE	0.1247	2.8434	150.0712
GLU_240@OE2	TYR_307@H	TYR_307@N	0.1231	2.8935	162.7057
ASP_153@OD1	ARG_316@HH11	ARG_316@NH1	0.1016	2.804	157.7267
ASP_245@OD2	TYR_308@HH	TYR_308@OH	0.0994	2.6853	162.1064
ARG_105@O	GLN_319@HE21	GLN_319@NE2	0.0956	2.8381	154.8202
ASP_245@O	TYR_310@HH	TYR_310@OH	0.0704	2.7293	160.2324
TYR_239@O	ARG_305@HH11	ARG_305@NH1	0.0682	2.837	163.8734
ASP_153@OD2	ARG_316@HH11	ARG_316@NH1	0.0681	2.7997	157.4653
GLN_110@OE1	ARG_311@H	ARG_311@N	0.0587	2.8657	159.6885
ASP_295@OD1	ARG_311@HH11	ARG_311@NH1	0.0546	2.8361	142.1695
ASN_231@OD1	ARG_305@HH12	ARG_305@NH1	0.0519	2.8318	151.9943
THR_292@OG1	ARG_311@HH11	ARG_311@NH1	0.0507	2.867	149.6515
THR_199@O	GLN_306@HE22	GLN_306@NE2	0.0496	2.8493	160.7769
ASP_295@OD2	ARG_311@HH12	ARG_311@NH1	0.0428	2.7513	153.1933
ASN_238@OD1	ARG_305@H3	ARG_305@N	0.0369	2.8308	152.7538
GLN_107@OE1	HIE_309@HE2	HIE_309@NE2	0.0364	2.8562	154.8376
ASP_295@OD1	ARG_311@HH12	ARG_311@NH1	0.0344	2.8235	152.5988
ASN_238@OD1	ARG_305@H2	ARG_305@N	0.0335	2.8386	153.0084
ASN_238@OD1	ARG_305@H1	ARG_305@N	0.0334	2.8376	152.4031
GLU_240@OE1	ARG_305@H1	ARG_305@N	0.0316	2.789	154.7962
GLU_240@OE1	ARG_305@H3	ARG_305@N	0.0304	2.7961	155.4412

TYR_182@OH	GLN_306@HE21	GLN_306@NE2	0.0289	2.8969	155.5248
VAL_104@HG12	ASP_318@H	ASP_318@N	0.0245	2.8471	150.1194
GLN_107@OE1	CYS_320@H	CYS_320@N	0.0181	2.8886	159.2411
GLU_240@OE1	ARG_305@H2	ARG_305@N	0.0162	2.8	154.2412
ASP_248@OD1	TYR_310@HH	TYR_310@OH	0.0157	2.686	161.9402
THR_292@HG1	ARG_311@HH11	ARG_311@NH1	0.0148	2.8498	141.3357
THR_201@HB	TYR_307@HD1	TYR_307@CD1	0.0144	2.9352	144.2208
PHE_294@HD2	ARG_311@HD3	ARG_311@CD	0.0142	2.9352	142.4346
GLU_240@OE2	GLN_306@HE22	GLN_306@NE2	0.0127	2.8244	163.3341
GLU_240@HG2	ARG_305@HG2	ARG_305@CG	0.0112	2.9429	141.0531
ARG_105@HB2	GLN_319@HB3	GLN_319@CB	0.0099	2.9445	143.0246
VAL_104@HG11	GLN_319@H	GLN_319@N	0.0094	2.8984	155.9604
GLN_110@OE1	HIE_309@HE2	HIE_309@NE2	0.0089	2.8597	151.3815
GLN_110@HG2	ARG_311@HD2	ARG_311@CD	0.0081	2.9419	143.2248
ASP_248@OD2	TYR_310@HH	TYR_310@OH	0.008	2.7026	161.6591
GLN_107@OE1	GLN_319@HE22	GLN_319@NE2	0.008	2.8583	161.114
GLU_240@HG2	ARG_305@HD2	ARG_305@CD	0.0072	2.9325	142.2131
GLN_110@HE21	GLN_319@HA	GLN_319@CA	0.0071	2.862	144.9203
ASN_238@OD1	ARG_305@HE	ARG_305@NE	0.007	2.8415	152.7091
GLU_240@OE1	ARG_305@HA	ARG_305@CA	0.0069	2.9611	140.6561
ASN_238@OD1	ARG_305@HH21	ARG_305@NH2	0.0067	2.8181	155.3648
PHE_294@HD1	ARG_311@HD3	ARG_311@CD	0.0066	2.933	142.4085
GLN_107@HG3	CYS_320@H	CYS_320@N	0.0061	2.8605	151.371
ASP_245@OD2	LYS_313@HZ2	LYS_313@NZ	0.0054	2.7926	156.4654
GLU_240@OE2	ARG_305@H1	ARG_305@N	0.0052	2.7625	155.1593
ALA_234@O	ARG_305@HH21	ARG_305@NH2	0.0052	2.8634	147.1161
ASP_245@OD2	LYS_313@HZ1	LYS_313@NZ	0.0052	2.7728	154.3983
PHE_294@HB2	TYR_312@HB2	TYR_312@CB	0.0052	2.9606	144.5844
ASN_238@O	GLN_306@HE21	GLN_306@NE2	0.0052	2.8905	154.7032
THR_201@HG1	TYR_307@HB3	TYR_307@CB	0.0051	2.9174	143.4791

6.4.5. Binding Free energy (BFE) and per residue energy decomposition (PRED) analysis

Using the MM-GBSA method, the binding free energies of the Mpro-peptide2 and Mpro-peptide4 complexes were determined from the last 10 ns of the MD simulation after the system reached equilibrium. The MM-GBSA technique employs a continuum solvent approach to calculate the binding free energies of a system; hence, the values listed below indicate only the relative binding free energy rather than absolute or total binding energy.

The total binding free energy determined for the Mpro-peptide2 complex and Mpro-peptide4 complex along with the energy components were summarized in **Tables 6.13 and 6.14**. From Table 6.13 and 6.14, it can be seen Mpro-peptide2 complex (GB_{TOT} = -72.85 kcal/mol, was energetically more favourable than the Mpro-peptide4 complex (GB_{TOT} = -46.36 kcal/ mol). Tables 6.13 and 6.14 show that all BFE

components contributed to Mpro and peptide binding to form the Mpro-peptide2 and Mpro-peptide4 complexes.

Table 6.13. *Binding free energies (kcal/mol) and its components of Mpro-peptide2 complex obtained using MM-GBSA approach.*

Energy Components	**$\Delta G_{(Mpro\text{-}peptide2)} - [\Delta G_{Mpro} + \Delta G_{peptide2}]$ (kcal/mol)**	
	Average	**std. dev. (±)**
VDW	-116.6537	4.9128
ELE	-329.8182	13.4203
GB	390.1802	12.3627
GBSUR	-16.5596	0.2869
GAS	-446.4719	13.6733
GBSOL	373.6206	12.3078
ΔG_{GBTOT}	**-72.85**	4.9772

Final estimated binding free energy (ΔG_{GBTOT})

Table 6.14. *Binding free energies (kcal/mol) and its components of Mpro-peptide4 complex obtained using MM-GBSA approach.*

Energy Components	**$\Delta G_{(Mpro\text{-}peptide4)} - [\Delta G_{Mpro} + \Delta G_{peptide4}]$ (kcal/mol)**	
	Average	**std. dev. (±)**
VDW	-70.0054	3.5450
ELE	-443.2822	12.9002
GB	477.6285	11.5000
GBSUR	-10.7086	0.3300
GAS	-513.2876	12.9632
GBSOL	466.9198	11.4341
ΔG_{GBTOT}	**-46.36**	5.0966

Final estimated binding free energy (ΔG_{GBTOT})

In order to gain insight into how each amino acid residue contributes to the overall protein-peptide interaction, PRED values were also computed. In this analysis, in order to identify the key residues between the Mpro and the peptide, the total binding energy was decomposed into individual residues. Essential residues with the binding energy value below -1.00 kcal/mol are shown in **Figure 6.13 and 6.14**. The residues that contribute the highest energy for Mpro-peptide2 complex are ASP 295, PHE 294, GLU 240, GLN110, ASP 153, ILE 249, ILE 152, THR 292, PRO 293, PHE 112 from the Mpro and GLN 308, TYR 310, ARG 316, TYR 309, TYR 314, TYR 312, HIE 311, GLU 306 from the peptide2 while the highest energy contributing residues in Mpro-peptide4 complex comes from ASP 295, ASN

231, TYR 239, HIE 246, ILE 249, THR 292, GLU 240, PHE 294, PRO 241, VAL 202 for Mpro and TYR 307, TYR 308, GLN 306, TYR 110, ASP 318, TYR 312, CYS 320, ARG 311 for the peptide4.

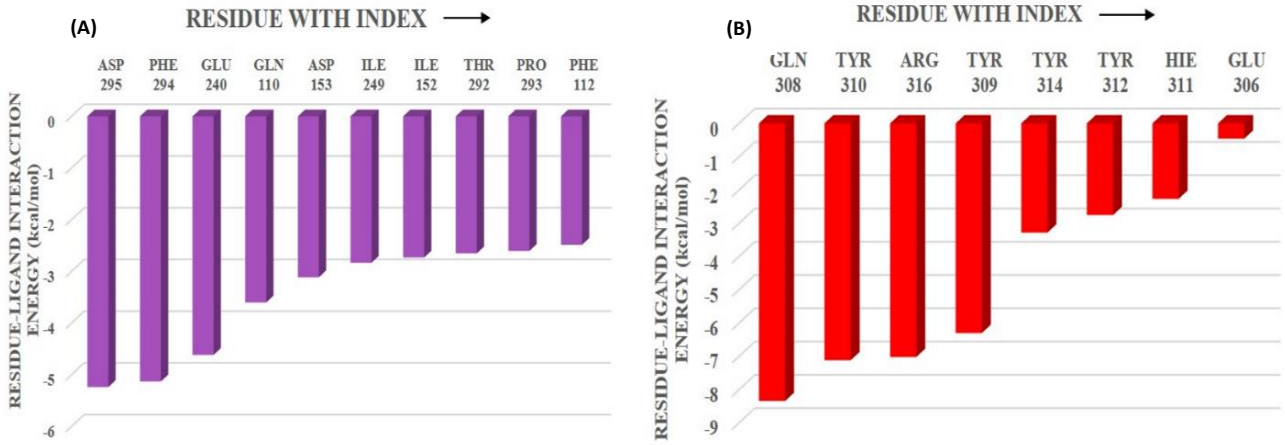

Figure 6.13. *Decomposition of binding free energy (kcal/mol) on per residue basis for Mpro binding to peptide2 obtained using MM-GBSA approach for* ***(A)*** *Mpro (violet) and* ***(B)*** *peptide2 (Red)*

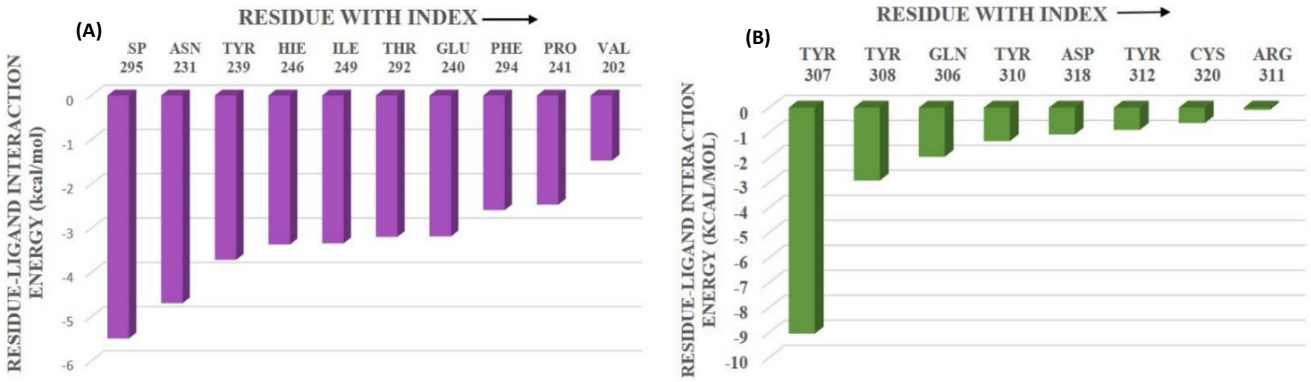

Figure 6.14. *Decomposition of binding free energy (kcal/mol) on per residue basis for Mpro binding to peptide4 obtained using MM-GBSA approach for* ***(A)*** *Mpro (violet)* ***(B)*** *peptide4 (green)*

6.5. Conclusion:

Even though several SARS-CoV-2 vaccinations have been established, the development of appropriate COVID-19 therapies is still essential as there is no recognized causative therapy or treatment so far. This study mainly involves designing of peptides against the Main protease (3CLpro) which is considered to be a potential drug targets for SARS-CoV-2 and our study is completely based on in-silico approach. Even though a significant number of small molecules or peptide inhibitors has been developed, there is

still a need to design molecules or peptides that may affect the functioning of the target molecule. According to literature, we found one high-confidence interaction between the main protease and the histone deacetylase 2 (HDAC2). Based on the interacting residues between the Mpro and HDAC2 we have designed the peptides. Among the 13 designed peptides, two peptides (peptide 2 and peptide 4) were screened out based on preliminary in-silico analysis (Toxicity, binding affinity, interaction study) and then were subjected to MD simulation for further analysis. On interpreting the RMSD and RMSF results of the two complex system (Mpro-peptide2 and Mpro-peptide4) and comparing it with the Mpro Apoprotein we found that the relative stability of the Mpro increases upon binding to the peptides. When compared the Mpro-peptide2 complex to the Mpro-peptide4 complex, it was found that the former had a higher number of intermolecular hydrogen bonds, which may account for its increased stability. We also performed the binding free energy analysis to check the affinity between the Mpro and the peptides. The binding free energy was found to be indeed high (GB_{TOT}= -72.85 kcal/mol) in case of the Mpro-peptide2 complex in comparison with Mpro-peptide4 complex (GB_{TOT} = -46.36 kcal/mol). Our findings showed that Mpro attains a higher stability when bound to the peptides and it was found that each of the designed peptides bind to the Mpro with strong affinity. These findings could aid in the development of novel SARS-CoV-2 Mpro peptide inhibitors.

6.6. Bibliography:

[1]. Hu, Q., Xiong, Y., Zhu, G. H., Zhang, Y. N., Zhang, Y. W., Huang, P., and Ge, G. B. The SARS-CoV-2 main protease (Mpro): Structure, function, and emerging therapies for COVID-19. *Medicine Communications*, 3(3): e151, 2022, https://doi.org/10.1002/mco2.151

[2]. WHO coronavirus disease (covid-19) dashboard. *Bangladesh Physiotherapy Journal*, 10(1), 2020. https://doi.org/10.46945/bpj.10.1.03.01

[3]. Mengist, H.M., Dilnessa, T., and Jin, T. Structural Basis of Potential Inhibitors Targeting SARS-CoV-2 Main Protease. *Frontiers in Chemistry*, 9: 622898, 2021. https://doi.org/10.3389/fchem.2021.622898.

[4]. Das, C., Das, D., and Mattaparthi, V. S. K. Computational Investigation on the Efficiency of Small Molecule Inhibitors Identified from Indian Spices against SARS-CoV-2 Mpro. *Biointerface Research in Applied Chemistry*, 13(3): 235, 2023**.** https://doi.org/10.33263/BRIAC133.235

[5]. Khailany, R. A., Safdar, M., and Ozaslan, M. Genomic characterization of a novel SARS-CoV-2. *Gene reports*, 19, 100682, 2020. https://doi.org/10.1016/j.genrep.2020.100682

[6]. Hegyi, A., and Ziebuhr, J. Conservation of substrate specificities among coronavirus main proteases.

The Journal of general virology, 83: 595–599, 2002. https://doi.org/10.1099/0022-1317-83-3-595

[7]. Anand, K., Ziebuhr, J., Wadhwani, P., Mesters, J. R., and Hilgenfeld, R. Coronavirus main proteinase (3CLpro) structure: basis for design of anti-SARS drugs. *Science*, 300(5626), 1763–1767, 2003. https://doi.org/10.1126/science.1085658

[8]. Hilgenfeld, R. From SARS to MERS: crystallographic studies on coronaviral proteases enable antiviral drug design. *The FEBS Journal*, 281(18): 4085-4096, 2014. https://doi.org/10.1111/febs.12936

[9]. Lu, L., Su, S., Yang, H., and Jiang, S. Antivirals with common targets against highly pathogenic viruses. *Cell*, 184(6): 1604–1620, 2021. https://doi.org/10.1016/j.cell.2021.02.013

[10]. Hu, B., Guo, H., Zhou, P., and Shi, Z.-L. Characteristics of SARS-COV-2 and COVID-19. *Nature Reviews Microbiology*, 20(5): 315–315, 2022. https://doi.org/10.1038/s41579-022-00711-2

[11]. Mikitsh, J.L., and Chacko, A.M. Pathways for small molecule delivery to the central nervous system across the blood-brain barrier. *Perspectives in Medicinal Chemistry*, 16(6): 11-24, 2014. https://doi.org/10.4137/PMC.S13384

[12]. Goodwin, D., Simerska, P., and Toth, I. Peptides as therapeutics with enhanced bioactivity. *Current medicinal chemistry*, 19(26): 4451–4461, 2012. https://doi.org/10.2174/092986712803251548

[13]. Zang, Y., Su, M., Wang, Q., Cheng, X., Zhang, W., Zhao, Y., Chen, T., Jiang, Y., Shen, Q., Du, J., Tan, Q., Wang, P., Gao, L., Jin, Z., Zhang, M., Li, C., Zhu, Y., Feng, B., Tang, B., Xie, H., Wang, M.W., Zheng, M., Pan, X., Yang, H., Xu, Y., Wu, B., Zhang, L., Rao, Z., Yang, X., Jiang, H., Xiao, G., Zhao, Q., and Li, J. High-throughput screening of SARS-CoV-2 main and papain-like protease inhibitors. *Protein & cell*, 14(1): 17–27, 2023. https://doi.org/10.1093/procel/pwac016

[14]. Owen, D. R., Allerton, C. M. N., Anderson, A. S., Aschenbrenner, L., Avery, M., Berritt, S., Boras, B., Cardin, R. D., Carlo, A., Coffman, K. J., Dantonio, A., Di, L., Eng, H., Ferre, R., Gajiwala, K. S., Gibson, S. A., Greasley, S. E., Hurst, B. L., Kadar, E. P., Kalgutkar, A. S., and Zhu, Y. An oral SARS-CoV-2 Mpro inhibitor clinical candidate for the treatment of COVID-19. *Science*, 374(6575): 1586–1593, 2021. https://doi.org/10.1126/science.abl4784

[15]. Beigel, J. H., Tomashek, K. M., Dodd, L. E., Mehta, A. K., Zingman, B. S., Kalil, A. C., Hohmann, E., Chu, H. Y., Luetkemeyer, A., Kline, S., Lopez de Castilla, D., Finberg, R. W., Dierberg, K., Tapson, V., Hsieh, L., Patterson, T. F., Paredes, R., Sweeney, D. A., Short, W. R., and Touloumi, G. Remdesivir for the Treatment of Covid-19 - Final Report. *The New England journal of medicine*, 383(19): 1813–1826, 2020. https://doi.org/10.1056/NEJMoa2007764

[16]. Hosseinzadeh, M. H., hamshirian, A., and Ebrahimzadeh, M. A. Dexamethasone vs Covid-19: An

experimental study in line with the preliminary findings of a large trial. *International journal of clinical practice*, 75(6): e13943, 2020. https://doi.org/10.1111/ijcp.13943

[17]. Nangaku, M., Kadowaki, T., Yotsuyanagi, H., Ohmagari, N., Egi, M., Sasaki, J., Sakamoto, T., Hasegawa, Y., Ogura, T., Chiba, S., Node, K., Suzuki, R., Yamaguchi, Y., Murashima, A., Ikeda, N., Morishita, E., Yuzawa, K., Moriuchi, H., Hayakawa, S., Nishi, D., and Fujino, Y. The Japanese Medical Science Federation COVID-19 Expert Opinion English Version. *JMA journal*, 4(2): 148–162, 2021. https://doi.org/10.31662/jmaj.2021-0002

[18]. Andreoni, M., Sticchi, L., Nozza, S., Sarmati, L., Gori, A., and Tavio, M., Society for Infectious and Tropical Diseases (SIMIT). Recommendations of the Italian society for infectious and tropical diseases (SIMIT) for adult vaccinations. *Human vaccines & Immunotherapeutics*, 17(11): 4265–4282, 2021. https://doi.org/10.1080/21645515.2021.1971473

[19]. Zhu K. W. Deuremidevir and Simnotrelvir-Ritonavir for the Treatment of COVID-19. *ACS pharmacology & translational science*, 6(9): 1306–1309, 2023. https://doi.org/10.1021/acsptsci.3c00134

[20]. Williamson, B. N., Feldmann, F., Schwarz, B., Meade-White, K., Porter, D. P., Schulz, J., van Doremalen, N., Leighton, I., Yinda, C. K., Pérez-Pérez, L., Okumura, A., Lovaglio, J., Hanley, P. W., Saturday, G., Bosio, C. M., Anzick, S., Barbian, K., Cihlar, T., Martens, C., Scott, D. P., and de Wit, E. Clinical benefit of remdesivir in rhesus macaques infected with SARS-CoV-2. *Nature*, 585(7824): 273–276, 2020. https://doi.org/10.1038/s41586-020-2423-5

[21]. Wahl, A., Gralinski, L.E., Johnson, C.E., Yao, W., Kovarova, M., Dinnon, K.H., Liu, H., Madden, V.J., Krzystek, H.M., De, C., White, K.K., Gully, K., Schäfer, A., Zaman, T., Leist, S.R., Grant, P.O., Bluemling, G.R., Kolykhalov, A.A., Natchus, M.G., Askin, F.B., Painter, G., Browne, E.P., Jones, C.D., Pickles, R.J., Baric, R.S., and Garcia, J.V. SARS-CoV-2 infection is effectively treated and prevented by EIDD-2801. *Nature*, 591(7850):451-457, 2021. https://doi.org/10.1038/s41586-021-03312-w

[22]. Xie, Y., Yin, W., Zhang, Y., Shang, W., Wang, Z., Luan, X., Tian, G., Aisa, H. A., Xu, Y., Xiao, G., Li, J., Jiang, H., Zhang, S., Zhang, L., Xu, H. E., and Shen, J. Design and development of an oral remdesivir derivative VV116 against SARS-CoV-2. *Cell research*, 31(11): 1212–1214, 2021. https://doi.org/10.1038/s41422-021-00570-1

[23]. Zhang, J. L., Li, Y. H., Wang, L. L., Liu, H. Q., Lu, S. Y., Liu, Y., Li, K., Liu, B., Li, S. Y., Shao, F. M., Wang, K., Sheng, N., Li, R., Cui, J. J., Sun, P. C., Ma, C. X., Zhu, B., Wang, Z., Wan, Y. H., Yu, S. S., and Jiang, J. D. Azvudine is a thymus-homing anti-SARS-CoV-2 drug effective in treating COVID-19 patients. *Signal transduction and targeted therapy*, 6(1): 414, 2021. https://doi.org/10.1038/s41392-021-00835-6

[24]. Unoh,Y., Uehara, S., Nakahara, K., Nobori, H., Yamatsu, Y., Yamamoto, S., Maruyama, Y., Taoda, Y., Kasamatsu, K., Suto, T., Kouki, K., Nakahashi, A., Kawashima, S., Sanaki, T., Toba, S., Uemura, K., Mizutare, T., Ando, S., Sasaki,M., Orba, Y., Sawa, H., Sato, A., Sato, T., Kato, T., and Tachibana. Y. Discovery of S-217622, a Noncovalent Oral SARS-CoV-2 3CL Protease Inhibitor Clinical Candidate for Treating COVID-19. *Journal of Medicinal Chemistry*, 65(9): 6499-6512, 2022. https://doi.org/10.1021/acs.jmedchem.2c00117

[25]. Yan, V. C., and Muller, F. L. Why Remdesivir Failed: Preclinical Assumptions Overestimate the Clinical Efficacy of Remdesivir for COVID-19 and Ebola. *Antimicrobial agents and chemotherapy*, 65(10): e0111721, 2021. https://doi.org/10.1128/AAC.01117-21

[26]. Heilmann, E., Costacurta, F., Moghadasi, S. A., Ye, C., Pavan, M., Bassani, D., Volland, A., Ascher, C., Weiss, A. K. H., Bante, D., Harris, R. S., Moro, S., Rupp, B., Martinez-Sobrido, L., and von Laer, D. SARS-CoV-2 3CLpro mutations selected in a VSV-based system confer resistance to nirmatrelvir, ensitrelvir, and GC376. *Science translational medicine*, 15(678): eabq7360, 2023. https://doi.org/10.1126/scitranslmed.abq7360

[27]. Noske, G. D., de Souza Silva, E., de Godoy, M. O., Dolci, I., Fernandes, R. S., Guido, R. V. C., Sjö, P., Oliva, G., and Godoy, A. S. Structural basis of nirmatrelvir and ensitrelvir activity against naturally occurring polymorphisms of the SARS-CoV-2 main protease. *The Journal of biological chemistry*, 299(3): 103004, 2023. https://doi.org/10.1016/j.jbc.2023.103004

[28]. Jochmans, D., Liu, C., Donckers, K., Stoycheva, A., Boland, S., Stevens, S.K., De Vita, C., Vanmechelen, B., Maes, P., Trüeb, B., Ebert, N., Thiel, V., De Jonghe, S., Vangeel, L., Bardiot, D., Jekle, A., Blatt, L.M., Beigelman, L., Symons, J.A., Raboisson, P., Chaltin, P., Marchand, A., Neyts, J., Deva, l. J., and Vandyck, K. The substitutions L50F, E166A and L167F in SARS-CoV-2 3CLpro are selected by a protease inhibitor *in vitro* and confer resistance to nirmatrelvir. *BioRxiv*, 2022.06.07.495116, 2022. https://doi.org/10.1101/2022.06.07.495116

[29]. Iketani, S., Mohri, H., Culbertson, B., Hong, S. J., Duan, Y., Luck, M. I., Annavajhala, M. K., Guo, Y., Sheng, Z., Uhlemann, A. C., Goff, S. P., Sabo, Y., Yang, H., Chavez, A., and Ho, D. D. Multiple pathways for SARS-CoV-2 resistance to nirmatrelvir. *Nature*, 613(7944), 558–564, 2023. https://doi.org/10.1038/s41586-022-05514-2

[30]. Sasi, V. M., Ullrich, S., Ton, J., Fry, S. E., Johansen-Leete, J., Payne, R. J., Nitsche, C., and Jackson, C. J. Predicting Antiviral Resistance Mutations in SARS-CoV-2 Main Protease with Computational and Experimental Screening. *Biochemistry*, 61(22): 2495–2505, 2022. https://doi.org/10.1021/acs.biochem.2c00489

[31]. Rambaut, A., Holmes, E. C., O'Toole, Á., Hill, V., McCrone, J. T., Ruis, C., du Plessis, L., Pybus, O. G. A dynamic nomenclature proposal for SARS-COV-2 lineages to assist genomic epidemiology. *Nature Microbiology*, 5(11): 1403–1407, 2020. https://doi.org/10.1038/s41564-020-0770-5

[32]. Gordon, D.E., Jang, G.M., Bouhaddou, M., Xu, J., Obernier, K., White, K.M., O'Meara, M.J., Rezelj, V.V., Guo, J.Z., Swaney, D.L., Tummino, T.A., Hüttenhain, R., Kaake, R.M., Richards, A.L., Tutuncuoglu, B., Foussard, H., Batra, J., Haas, K., Modak, M., Kim, M., Haas, P., Polacco, B.J., Braberg, H., Fabius, J.M., Eckhardt, M., Soucheray, M., Bennett, M.J., Cakir, M., McGregor, M.J, Li, Q., Meyer, B., Roesch, F., Vallet, T., Mac Kain A., Miorin, L., Moreno, E., Naing, Z.Z.C., Zhou, Y., Peng, S., Shi, Y., Zhang, Z., Shen, W., Kirby, I.T., Melnyk, J.E., Chorba, J.S., Lou, K., Dai, S.A., Barrio-Hernandez, I., Memon, D., Hernandez-Armenta, C., Lyu, J., Mathy, C.J.P., Perica, T., Pilla, K.B., Ganesan, S.J., Saltzberg, D.J., Rakesh, R., Liu, X., Rosenthal, S.B., Calviello, L., Venkataramanan, S., Liboy-Lugo, J., Lin, Y., Huang, X.P., Liu, Y., Wankowicz, S.A., Bohn, M., Safari, M., Ugur, F.S., Koh, C., Savar, N.S., Tran, Q.D., Shengjuler, D., Fletcher, S.J., O'Neal, M.C., Cai, Y., Chang, J.C.J., Broadhurst, D.J., Klippsten, S., Sharp, P.P., Wenzell, N.A., Kuzuoglu-Ozturk, D., Wang, H.Y., Trenker, R., Young, J.M., Cavero, D.A., Hiatt, J., Roth, T.L., Rathore, U., Subramanian, A., Noack, J., Hubert, M., Stroud, R.M., Frankel, A.D., Rosenberg, O.S., Verba, K.A., Agard, D.A., Ott, M., Emerman, M., Jura, N., von Zastrow, M., Verdin, E., Ashworth, A., Schwartz, O., d'Enfert, C., Mukherjee, S., Jacobson, M., Malik, H.S., Fujimori, D.G., Ideker, T., Craik, C.S., Floor, S.N., Fraser, J.S., Gross, J.D., Sali, A., Roth, B.L., Ruggero, D., Taunton, J., Kortemme, T., Beltrao, P., Vignuzzi, M., García-Sastre, A., Shokat, K.M., Shoichet, B.K., and Krogan, N.J. A SARS-CoV-2 protein interaction map reveals targets for drug repurposing. *Nature*, 583(7816): 459-468, 2020. https://doi.org/10.1038/s41586-020-2286-9

[33]. Vajda, S., Yueh, C., Beglov, D., Bohnuud, T., Mottarella, S. E., Xia, B., Hall, D. R., and Kozakov, D. New additions to the ClusPro server motivated by CAPRI. *Proteins*, 85(3): 435–444, 2017. https://doi.org/10.1002/prot.25219

[34]. Kozakov, D., Hall, D. R., Xia, B., Porter, K. A., Padhorny, D., Yueh, C., Beglov, D., and Vajda, S. The ClusPro web server for protein-protein docking. *Nature protocols*, 12(2): 255–278, 2017. https://doi.org/10.1038/nprot.2016.169

[35]. Yan Y, Tao H, He J, and Huang SY. The HDOCK server for integrated protein-protein docking. *Nature Protocols*, 15(5):1829-1852, 2020.https://doi.org/10.1038/s41596-020-0312-x.

[36]. Yan, Y., Zhang, D., Zhou, P., Li, B., and Huang, S. Y. HDOCK: a web server for protein-protein and protein-DNA/RNA docking based on a hybrid strategy. *Nucleic acids research*, 45(W1): W365–W373, 2017. https://doi.org/10.1093/nar/gkx407

[37]. Eisenberg, D., Lüthy, R., and Bowie, J. U. VERIFY3D: assessment of protein models with three-dimensional profiles. *Methods in enzymology*, 277: 396–404, 1997. https://doi.org/10.1016/s0076-6879(97)77022-8

[38]. Colovos, C., and Yeates, T. O. Verification of protein structures: patterns of nonbonded atomic interactions. *Protein science: a publication of the Protein Society*, 2(9): 1511–1519, 1993. https://doi.org/10.1002/pro.5560020916

[39]. Laskowski, R. A., Hutchinson, E. G., Michie, A. D., Wallace, A. C., Jones, M. L., and Thornton, J. M. PDBsum: A Web-based database of summaries and analyses of all PDB structures. *Trends in Biochemical Sciences*, 22(12): 488–490, 1997. https://doi.org/10.1016/s0968-0004(97)01140-7

[40]. Badaczewska-Dawid, A. E., Nithin, C., Wroblewski, K., Kurcinski, M., and Kmiecik, S. MAPIYA contact map server for identification and visualization of molecular interactions in proteins and biological complexes. *Nucleic acids research*, 50(W1): W474–W482, 2022. https://doi.org/10.1093/nar/gkac307

[41]. Kurcinski, M., Jamroz, M., Blaszczyk, M., Kolinski, A., and Kmiecik, S. CABS-dock web server for the flexible docking of peptides to proteins without prior knowledge of the binding site. *Nucleic acids research*, 43(W1): W419–W424, 2015. https://doi.org/10.1093/nar/gkv456

[42]. Blaszczyk, M., Kurcinski, M., Kouza, M., Wieteska, L., Debinski, A., Kolinski, A., and Kmiecik, S. Modeling of protein-peptide interactions using the CABS-dock web server for binding site search and flexible docking. *Methods (San Diego, Calif.)*, 93: 72–83, 2016. https://doi.org/10.1016/j.ymeth.2015.07.004

[43]. Wei, L., Ye, X., Sakurai, T., Mu, Z., and Wei, L. ToxIBTL: prediction of peptide toxicity based on information bottleneck and transfer learning. *Bioinformatics*, 38(6): 1514–1524, 2022. https://doi.org/10.1093/bioinformatics/btac006

[44]. Xue, L. C., Rodrigues, J. P., Kastritis, P. L., Bonvin, A. M., and Vangone, A. Prodigy: A web server for predicting the binding affinity of protein–protein complexes. *Bioinformatics*, 32(23): 3676–3678, 2016. https://doi.org/10.1093/bioinformatics/btw514

[45]. Eberle, R. J., Sevenich, M., Gering, I., Scharbert, L., Strodel, B., Lakomek, N. A., Santur, K., Mohrlüder, J., Coronado, M. A., and Willbold, D. Discovery of All-d-Peptide Inhibitors of SARS-CoV-2 3C-like Protease. *ACS chemical biology*, 18(2): 315–330, 2023. https://doi.org/10.1021/acschembio.2c00735

[46]. Xiong, G., Wu, Z., Yi, J., Fu, L., Yang, Z., Hsieh, C., Yin, M., Zeng, X., Wu, C., Chen, Hou, T., and Cao, D. ADMETlab 2.0: an integrated online platform for accurate and comprehensive predictions of ADMET properties. *Nucleic Acids Research*, 49: W5-W14, 2021. https://doi.org/10.1093/nar/gkab255

[47]. Tian, C., Kasavajhala, K., Belfon, K. A. A., Raguette, L., Huang, H., Migues, A. N., Bickel, J., Wang, Y., Pincay, J., Wu, Q., and Simmerling, C. ff19SB: Amino-Acid-Specific Protein Backbone Parameters Trained against Quantum Mechanics Energy Surfaces in Solution. *Journal of chemical theory and computation*,16(1): 528–552, 2020. https://doi.org/10.1021/acs.jctc.9b00591

[48]. Eduardo Sanabria-Chanaga, E., Betancourt-Conde, I., Hernández-Campos, A., Téllez-Valencia, A., and Castillo, R. In silico hit optimization toward AKT inhibition: fragment-based approach, molecular docking and molecular dynamics study. *Journal of biomolecular structure & dynamics*, 37(16): 4301–4311, 2019. https://doi.org/10.1080/07391102.2018.1546618

[49]. Salomon-Ferrer, R., Gotz, A.W., Poole, D., Le Grand, S., and Walker, R.C. Routine microsecond molecular dynamics simulations with AMBER on GPUs. 2. Explicit solvent particle mesh Ewald. J*ournal of chemical theory and computation*, 9(9): 3878–3888, 2013. https://doi.org/10.1021/ct400314y.

[50]. Case, D.A., Cheatham, T.E., Darden, T., Gohlke, H., Luo, R., Merz, K.M., Onufriev, A., Simmerling, Z., Wang, B., and Woods, R. The Amber biomolecular simulation programs. *Journal of Computational Chemistry*, 26(16): 1668-1688, 2005. https://doi.org/10.1002/jcc.20290

[51]. Michael, F., Chen, L.Y, Chan, R, and Liang, H. TIP3P and TIP4P in Molecular Dynamics Simulations of Erythrocyte Aquaporins, *TACCSTER Proceedings*, 2020. http://dx.doi.org/10.26153/tsw/11475

[52]. Jorgensen, W.L., Chandrasekhar, J., Madura, J.D., Impey, R.W., and Klein, M.L. Comparison of simple potential functions for simulating liquid water. *The Journal of Chemical Physics*, 79 (2): 926–935, 1983. http://dx.doi.org/10.1063/1.445869

[53]. Darden, T., York, D., and Pedersen, L. Particle mesh Ewald: An N· log (N) method for Ewald sums in large systems. *The Journal of Chemical Physics*, 98 (12): 10089–10092, 1993. https://doi.org/10.1063/1.464397.

[54]. Ryckaert, J.P., Ciccotti, G., and Berendsen, H.J.C. Numerical integration of the cartesian equations of motion of a system with constraints: molecular dynamics of n-alkanes. *Journal of Computational Physics*, 23: 327−341, 1977. https://doi.org/10.1016/0021-9991(77)90098-5.

[55]. Berendsen, H.J., Postma, J.V., Van, G.W.F., DiNola, A.R.H.J., and Haak, J.R. Molecular dynamics with coupling to an external bath. *The Journal of Chemical Physics*, 81(8): 3684–3690, 1984. https://doi.org/10.1063/1.448118.

[56]. Roe, D.R., and Cheatham III, T.E. PTRAJ and CPPTRAJ: software for processing and analysis of molecular dynamics trajectory data. *Journal of chemical theory and computation*, 9(7): 3084–3095, 2013. https://doi.org/10.1021/ct400341p.

[57]. Chen, F., Liu, H., Sun, H., Pan, P., Li, Y., Li, D., and Hou, T. Assessing the performance of the MM/PBSA and MM/GBSA methods. 6. Capability to predict protein–protein binding free energies and re-rank binding poses generated by protein–protein docking. *Physical Chemistry Chemical Physics*, 18(32): 22129-22139, 2016, https://doi.org/10.1039/c6cp03670h.

[58]. Genheden, S., and Ryde, U. The MM/PBSA and MM/GBSA methods to estimate ligand-binding affinities. *Expert opinion on drug discovery*, 10(5): 449–461, 2015. http://doi.org/10.1517/17460441.2015.1032936.

[59]. Chen, J., Yin, B., Pang, L., Wang, W., Zhang, J.Z., and Zhu, T. Binding modes and conformational changes of FK506 binding protein 51 induced by inhibitor bindings: insight into molecular mechanisms based on multiple simulation technologies. *Journal of biomolecular structure & dynamics*, *38*(7), 2141–2155, 2020. https://doi.org/10.1080/07391102.2019.1624616.

[60]. Du, Q., Qian, Y., Yao, X., and Xue, W. Elucidating the tight-binding mechanism of two oral anticoagulants to factor Xa by using induced-fit docking and molecular dynamics simulation. *Journal of biomolecular structure & dynamics*, 38(2): 625–633, 2020. https://doi.org/10.1080/07391102.2019.1583605

[61]. Gao, J., Wang, Y., Chen, Q., and Yao, R. Integrating molecular dynamics simulation and molecular mechanics/generalized Born surface area calculation into pharmacophore modeling: a case study on the

proviral integration site for Moloney murine leukemia virus (Pim)-1 kinase inhibitors. *Journal of Biomolecular Structure and Dynamics*, 38: 1-10, 2020. http://doi.org/10.1080/07391102.2019.1571946.

[62]. Joshi, T., Joshi, T., Sharma, P., Chandra, S., and Pande, V. Molecular docking and molecular dynamics simulation approach to screen natural compounds for inhibition of Xanthomonas oryzae pv. Oryzae by targeting Peptide Deformylase. *Journal of biomolecular structure & dynamics*, 39(3): 823–840, 2021. https://doi.org/10.1080/07391102.2020.1719200

[63]. Sk, M.F., Roy, R., and Kar, P. Exploring the potency of currently used drugs against HIV-1 protease of subtype D variant multiscale simulations. *Journal of Biomolecular Structure and Dynamics*, 39(3): 988-1003, 2020. https://doi.org/10.1080/07391102.2020.1724196.

[64]. Sun, H., Duan, L., Chen, F., Liu, H., Wang, Z., Pan, P., Zhu, F., Zhang, J.Z.H., and Hou, T. Assessing the performance of MM/PBSA and MM/GBSA methods. 7. Entropy effects on the performance of endpoint binding free energy calculation approaches. *Physical Chemistry Chemical Physics*, 20(21): 14450-14460, 2018. https://doi.org/10.1039/C7CP07623A. Tian, S., Ji, C., John Z., and Zhang, H. Molecular basis of SMAC-XIAP binding and the effect of electrostatic polarization. *Journal of Biomolecular Structure and Dynamics*, 39(2): 743-752, 2021. https://doi.org/10.1080/07391102.2020.1713892

[65]. Wan, Y., Guan, S., Qian, M., Huang, H., Han, F., Wang, S., and Zhang, H. Structural basis of fullerene derivatives as novel potent inhibitors of protein acetylcholinesterase without catalytic active site interaction: insight into the inhibitory mechanism through molecular modeling studies. *Journal of biomolecular structure & dynamics*, 38(2): 410–425, 2020. https://doi.org/10.1080/07391102.2019.1576543

[66]. Wang, E., Sun, H., Wang, J., Wang, Z., Liu, H., Zhang, J.Z.H., and Hou, T. End-Point Binding Free Energy Calculation with MM/PBSA and MM/GBSA: Strategies and Applications in Drug Design. *Chemical Reviews*, 119: 9478- 9508, 2019. https://doi.org/10.1021/acs.chemrev.9b00055.

[67]. Zhang, W., Yang, F., Ou, D., Lin, G., Huang, A., Liu, N., and Li, P. Prediction, docking study and molecular simulation of 3D DNA aptamers to their targets of endocrine disrupting chemicals. *Journal of biomolecular structure & dynamics*, 37(16): 4274–4282, 2019. https://doi.org/10.1080/07391102.2018.1547222.

[68]. Das, C., Das, D., and Mattaparthi, V.S.K. Effect of Mutations in the SARS-CoV-2 Spike RBD Region of Delta and Delta-Plus Variants on its Interaction with ACE2 Receptor Protein. *Letters in Applied NanoBioScience*, 12, 118, 2023. https://doi.org/10.33263/LIANBS124.118

[69]. Das, C., and Mattaparthi, V. S. K. Impact of Mutations in the SARS-CoV-2 Spike RBD Region of BA1 and BA2 Variants on its Interaction with ACE2 Receptor Protein. *Biointerface Research in. Applied Chemistry*, 13(4), 358, 2023. https://doi.org/10.33263/BRIAC134.358

[70]. Das, C., Hazarika, P.J., Deb, A., Joshi, P., Das, D., and Mattaparthi, V.S.K. Effect of Double Mutation (L452R and E484Q) in RBD of Spike Protein on its Interaction with ACE2 Receptor Protein. *Biointerface Research in. Applied Chemistry*, 13, 97, 2022. https://doi.org/10.33263/BRIAC131.097